1 **Wintertime aerosol chemical composition, volatility, and spatial variability in the greater**

2 **London area**

3 L. Xu[1], L.R. Williams[2], D.E. Young[3,*], J.D. Allan[3,4], H. Coe[3], P. Massoli[2], E. Fortner[2], P.

4 Chhabra[2,**], S. Herndon[2], W.A. Brooks[2], J.T. Jayne[2], D.R. Worsnop[2], A.C. Aiken[5], S. Liu[5,***], K.

5 Gorkowski[5,****], M.K. Dubey[5], Z.L. Fleming[6,7], S. Visser[8], A.S.H. Prevot[8], N.L. Ng[1,9]

6 [1]School of Chemical and Biomolecular Engineering, Georgia Institute of Technology, Atlanta, GA,

7 USA

8 [2]Aerodyne Research Inc., Billerica, MA, USA

9 [3]School of Earth, Atmospheric and Environmental Sciences, University of Manchester,

10 Manchester, UK

11 [4]National Centre for Atmospheric Science, University of Manchester, Manchester, UK

12 [5]Earth and Environmental Sciences Division, Los Alamos National Laboratory, Los Alamos, New

13 Mexico, USA.

14 [6]Department of Chemistry, University of Leicester, Leicester UK

15 [7]National Centre for Atmospheric Science, University of Leicester, Leicester, UK

16 [8]Laboratory of Atmospheric Chemistry, Paul Scherrer Institute, Villigen, Switzerland

17 [9]School of Earth and Atmospheric Sciences, Georgia Institute of Technology, Atlanta, GA, USA

18 [*]now at: Department of Environmental Toxicology, University of California, Davis, CA, USA

19 [**]now at: PerkinElmer Inc. Hopkinton, MA

20 [***]now at: Cooperative Institute for Research in the Environmental Sciences, University of

21 Colorado, Boulder, Colorado, USA.

22 [****]now at: Center for Atmospheric Particle Studies, Carnegie Mellon University, Pittsburgh, PA,

23 USA

24 Correspondence to N. L. Ng (ng@chbe.gatech.edu)

25

26

27

Abstract

28

29   The composition of PM_1 (particulate matter with diameter less than 1µm) in the greater

30   London area was characterized during the Clean Air for London (ClearfLo) project in winter 2012.

31   Two High-Resolution Time-of-Flight Aerosol Mass Spectrometers (HR-ToF-AMS) were

32   deployed at a rural site (Detling, Kent) and an urban site (North Kensington, London). The

33   simultaneous and high-temporal resolution measurements at the two sites provide a unique

34   opportunity to investigate the spatial distribution of PM_1. We find that the organic aerosol (OA)

35   concentration is comparable between the rural and urban sites, but the contribution from different

36   sources is distinctly different between the two sites. The concentration of solid fuel OA at the

37   urban site is about twice as high as at the rural site, due to elevated domestic heating in the urban

38   area. While the concentrations of oxygenated OA (OOA) are well-correlated between the two sites,

39   the OOA concentration at the rural site is almost twice that of the urban site. At the rural site, more

40   than 70% of the carbon in OOA is estimated to be non-fossil, which suggests that OOA is likely

41   related to aged biomass burning considering the small amount of biogenic SOA in winter. Thus, it

42   is possible that the biomass burning OA contributes a larger fraction of ambient OA in wintertime

43   than what previous field studies have suggested.

44   A suite of instruments was deployed downstream of a thermal denuder (TD) to investigate

45   the volatility of PM_1 species at the rural Detling site. After heating at 250°C in the TD, 40% of the

46   residual mass is OA, indicating the presence of non-volatile organics in the aerosol. Although the

47   OA associated with refractory black carbon (rBC, measured by a soot-particle aerosol mass

48   spectrometer) only accounts for <10% of the total OA (measured by a HR-ToF-AMS) at 250°C,

49   the two measurements are well-correlated, suggesting that the non-volatile organics have similar

50   sources or have undergone similar chemical processing as rBC in the atmosphere. Although the

51   atomic O:C ratio of OOA is substantially larger than that of solid fuel OA and hydrocarbon-like

52   OA, these three factors have similar volatility, which is inferred from the change in mass

53   concentration after heating at 120°C. Finally, we discuss the relationship between the mass fraction

54   remaining (MFR) of OA after heating in the TD and atomic O:C of OA and find that particles with

55   a wide range of O:C could have similar MFR after heating. This analysis emphasizes the

56   importance of understanding the distribution of volatility and O:C in bulk OA.

1 Introduction

Particulate matter (PM) concentration in the greater London area often exceeds European air quality limits, causing adverse effects on the health of habitants in this area (Harrison et al., 2012; Bohnenstengel et al., 2014). Therefore, it is critical to identify the PM sources in order to implement effective strategies to control ambient pollutants. The Clean Air for London (ClearfLo) project aimed to study boundary layer pollution in the greater London area through comprehensive measurements of meteorology, gaseous and particulate composition (Bohnenstengel et al., 2014). Multiple monitoring sites were set up in both urban and rural areas around London to quantify the urban increment in gas-phase and particle-phase pollutants.

Previous studies in the greater London area have repeatedly shown that the concentration of elemental carbon (EC) is higher in urban sites than rural sites due to elevated levels of primary emissions such as vehicle exhaust and wood smoke (Crilley et al., 2015; Yin et al., 2015). The origin of organic carbon (OC) at urban and rural sites is instead more challenging to elucidate considering the myriad of different OC sources. Based on the ratios among multiple tracers (e.g., EC/OC and levoglucosan/OC) from different sources, Crilley et al. (2015) estimated that the concentration of primary OC from vehicle emissions was higher in an urban area compared to a rural area in the UK. Many studies have applied the Chemical Mass Balance (CMB) model for OC apportionment (Yin et al., 2010; Crilley et al., 2015; Yin et al., 2015). However, due to the uncertainties in the source profiles and the number of organic tracers included in the model, the concentration of secondary OC is highly uncertain. In addition, OC measurements based on filter samples on a daily basis limit the temporal resolution of rural vs. urban comparisons.

Factor analysis via Positive Matrix factorization (PMF) of aerosol mass spectrometer (AMS) measurements is another widely used method to identify sources of organic aerosol (OA) (Jimenez et al., 2009; Lanz et al., 2007; Ng et al., 2010; Xu et al., 2015a). Based on factor analysis of AMS measurements around the world, Zhang et al. (2007) observed that the contribution of hydrocarbon-like OA (a surrogate for primary OA) to total OA decreased from urban sites to rural sites, but the oxygenated OA (a surrogate for secondary OA), showed the opposite trend. The authors also showed that the average OA concentration is substantially lower in rural sites than urban sites (2.8 vs. 7.6 $\mu g\ m^{-3}$). However, the trend observed in Zhang et al. (2007) needs to be

86 further verified since the urban vs. rural comparisons are not based on simultaneous measurements
87 between paired locations.

88   Comparison based on simultaneous measurements between different sites, especially
89 between rural and urban sites, is useful to identify regional and local sources of OA. For example,
90 by comparing concurrent AMS measurements of OA at multiple sites in the greater Atlanta area,
91 USA, Xu et al. (2015b) showed that the OA was spatially homogeneous and mainly regional in
92 summer, but the OA showed substantial spatial variability in winter. Based on PMF analysis of
93 AMS measurements, Crippa et al. (2013) investigated the correlation of various OA subtypes
94 between three urban sites located in a 20km-radius region in Paris, France during winter 2010. The
95 authors observed that the secondary OA factor had substantially better correlation between
96 different sites than the primary OA factors, including OA from vehicle, biomass burning, and
97 cooking. However, a rural vs. urban comparison was not performed in Crippa et al. (2013).

98   In addition to OA sources, the volatility of OA is an important property since it directly
99 determines the gas/particle partitioning. The thermal denuder (TD) has been used widely to
100 measure the aerosol volatility (An et al., 2007; Huffman et al., 2008; Saleh et al., 2012). Many
101 previous studies inferred the volatility from the mass fraction remaining (MFR) or volume fraction
102 remaining (VFR), which is calculated as the ratio of the species mass (or volume) concentration
103 after heating to an elevated temperature in the TD to the species mass (or volume) concentration
104 without heating (An et al., 2007; Huffman et al., 2009b; Jonsson et al., 2007; Lee et al., 2011;
105 Stanier et al., 2007; Grieshop et al., 2009b; Xu et al., 2014; Huffman et al., 2009a). Larger MFR
106 is used as an indication for lower volatility of aerosol. However, Saleh et al. (2011) suggested that
107 it is misleading to use MFR as an indication of volatility. This is mainly because the MFR is an
108 extensive parameter (which explicitly depends on the initial mass concentration) while aerosol
109 volatility is an intensive property (which depends only on chemical nature of the compounds in a
110 mixture). Instead of MFR, Saleh et al. (2011) presented that that change in mass concentration
111 when reaching equilibrium upon heating (i.e., ΔC) is an appropriate measure of volatility.

112   Although multiple previous studies have investigated the volatility of laboratory-generated
113 OA (An et al., 2007; Huffman et al., 2009b; Jonsson et al., 2007; Lee et al., 2011; Stanier et al.,
114 2007; Grieshop et al., 2009b; Xu et al., 2014), there are only limited studies on the volatility of
115 ambient OA, especially on the volatility of OA from different sources (Hildebrandt et al., 2010;

4

116   Huffman et al., 2009a; Massoli et al., 2015; Paciga et al., 2015). Previous studies have showed the

117   presence of non-volatile organics in the ambient aerosol even after heating to high temperatures

118   (i.e., 230 - 300°C) (Huffman et al., 2009a; Häkkinen et al., 2012; Poulain et al., 2014; Massoli et

119   al., 2015; Liu et al., 2015). However, the sources of non-volatile organics are uncertain. Häkkinen

120   et al. (2012) and Poulain et al. (2014) found that the non-volatile residuals correlated with

121   anthropogenic tracers, such as BC and polycyclic aromatic hydrocarbons (PAHs), implying that

122   the non-volatile species are possibly linked to anthropogenic emissions. However, in both studies,

123   the thermal-denuder (TD) was only applied upstream of a scanning mobility particle sizer (SMPS);

124   therefore the composition of remaining compounds was not directly measured but only conjectured.

125   Massoli et al. (2015) coupled a TD with a soot-particle AMS (SP-AMS) during measurements in

126   California. The authors observed the existence of refractory OA (i.e., detectable via laser

127   vaporization in the SP-AMS, but not detectable by vaporization at 600°C in the standard AMS),

128   which was present in the fresh urban air masses, but not in the aged air masses.

129   Many studies have used the degree of oxidation of OA, such as atomic O:C ratio and

130   oxidation state (OS) as a proxy for volatility. For example, two oxygenated OA factors with high

131   but different O:C ratio are often resolved from PMF analysis on AMS data. These two oxygenated

132   OA factors are often named semi-volatile OOA (SVOOA) and low-volatility OOA (LVOOA)

133   based on the volatility inferred from O:C values (Ng et al., 2010; Huang et al., 2010; Mohr et al.,

134   2012; Jimenez et al., 2009). In a laboratory study on toluene SOA, Hildebrandt Ruiz et al. (2014)

135   observed a linear relationship between OS and effective saturation concentration of the aerosol.

136   However, for both ambient measurements and laboratory studies, it is uncertain whether the O:C

137   or OS of bulk OA is a good indicator of volatility. In Mexico City and Riverside, CA, Huffman et

138   al. (2009a) showed that the O:C ratio of the thermally-denuded OA increased with TD heating

139   temperature, which suggests that the O:C is inversely correlated with the volatility of organic

140   aerosol (i.e., the residual OA with lower volatility after heating has a higher O:C). In contrast, only

141   a weak correlation between O:C and volatility was observed in Hildebrandt et al. (2010), who

142   measured the volatility of ambient OA in Finokalia, Greece. The authors found that between

143   thermally-denuded OA and ambient OA, the mass spectrum was similar and the difference in f_{44}

144   (i.e., fraction of organic signal at m/z 44, which has a linear correlation with O:C) was not

145   statistically significant. This indicates that the degree of oxidation does not change after

146   evaporation of relatively volatile species. In addition, various relationships between O:C and

147 volatility (inferred from the MFR) have been observed in previous laboratory studies on different
148 SOA systems (Grieshop et al., 2009b; Qi et al., 2010; Donahue et al., 2012; Kroll et al., 2009;
149 Tritscher et al., 2011; Xu et al., 2014). For example, Xu et al. (2014) observed that while the O:C
150 of isoprene SOA formed in the laboratory without additional NO remained fairly constant (~0.6)
151 during photochemical aging, the VFR increased over time. Grieshop et al. (2009b) showed that
152 during photochemical aging, OA from wood fires became more oxidized (i.e., O:C increases), but
153 the MFR remained constant. Donahue et al. (2012) studied the photochemical aging of α-pinene
154 ozonolysis SOA and observed that while the OA became more oxidized (i.e., O:C increases), the
155 VFR decreased with aging. The authors proposed that the photochemical aging produced both
156 relatively volatile products and more oxidized products, which broadened the volatility distribution
157 of the OA (Donahue et al., 2012). In summary, while SOA becomes progressively more oxidized
158 (i.e., O:C increases) during aging, the MFR or VFR exhibits different trends (i.e., increases, stays
159 constant, or decreases over time) for different SOA systems.

160   In this study, we performed simultaneous measurements at a rural site (Detling, Kent) and
161 an urban site (North Kensington, London) in the greater London area in winter 2012 using two
162 Aerodyne high resolution time-of-flight mass spectrometers (HR-ToF-AMS) (DeCarlo et al.,
163 2006). The comparison of the simultaneous, high temporal resolution measurements and the OA
164 source apportionment by PMF analysis provide insights into sources of wintertime OA in the
165 greater London area. Since biogenic emissions are low in winter, these measurements allow a more
166 direct evaluation of the contributions of anthropogenic emissions to OA formation. We also
167 deployed a thermal denuder upstream of a suite of instruments to directly characterize the non-
168 volatile residual at 250°C. Furthermore, we investigated the volatility of different OA sources and
169 systematically evaluated the relationship between O:C and OA volatility.

170 **2 Method**

171 2.1 Sampling sites and meteorological conditions

172   Measurements were performed as part of the Clean Air for London (ClearfLo) project. An
173 overview of the ClearfLo field campaign can be found in Bohnenstengel et al. (2014). The main
174 goal of the ClearfLo project was to study boundary layer pollution in the greater London area by
175 comprehensive measurements of meteorology, gaseous- and particulate composition. Multiple

176   monitoring sites were set up in both urban and rural areas and at different elevations (street and

177   elevated level) to perform year-long measurements across London. In addition, two intensive

178   observation periods (IOPs) were conducted during winter (January-February, 2012) and summer

179   (July-August, 2012). Data presented in this paper were collected at the Detling site and the North

180   Kensington (NK) site during the winter IOP. Figure 1 shows the locations of both sites. The NK

181   site (51.521055°N, 0.213432°W) is an urban background site located in a residential area, 7 km to

182   the west of central London. The Detling site (51.301931°N, 0.589494°E) is a rural site located on

183   a plateau (200 m a.s.l.), 45 km southeast of London. The closest road is about 150m (south), which

184   carries ~42,000 vehicles per day (www.dft.gov.uk/traffic-counts). The typical meteorological data

185   (temperature, relative humidity, and wind speed) at the Detling site are shown in Fig. S1a. The

186   campaign-average temperature was 6°C. In the diurnal variation, the highest temperature was ~8°C

187   at 14:00 and the lowest temperature was ~5°C at 07:00. The relative humidity was 83% on average.

188   The wind speed was 5.8 m s^{-1} on average, but it reached 10 m s^{-1} occasionally. The wind rose plot

189   is shown in Fig. S1b. The prevailing wind was from the northeast and the southwest.

190   2.2 Instrumentation

191   In the following discussions on instrumental setup and data analysis methods, we will focus

192   on the rural Detling site. For instruments deployed at the urban NK site, only the high-resolution

193   time-of-flight aerosol mass spectrometer (HR-ToF-AMS, Aerodyne) ambient measurements are

194   included in this study. The data analysis of HR-ToF-AMS at the urban site is similar to that at the

195   rural site, which will be discussed below. Details regarding the measurements at the NK site can

196   be found in Young et al. (2015a).

197   A suite of instruments was deployed at the Detling site to characterize both the gas-phase

198   and particle-phase composition. Instruments of interest to this study are shown in Fig. S2 and are

199   described below. Ambient particles were sampled through a PM$_{2.5}$ cyclone and then directed

200   through either a thermal denuder (denoted as TD line) or bypass line (denoted as bypass line)

201   before being analyzed by downstream instruments. The thermal denuder (TD, Aerodyne),

202   designed based on Huffman et al. (2008), consists of a 22" long stainless steel tube operated at

203   elevated temperatures (i.e., heated section), followed by a 24" section of activated charcoal held

204   at room temperature to adsorb the evaporated components from particles. The heating section was

205   operated at 120 and 250°C. The aerosol residence time in the heating section of the TD was 5.3 s

206   at the experimental flowrate rate (2.3 LPM determined by the sampling rate of instruments

207   downstream of the TD). Caution is required when comparing the results between different studies

208   with a TD because the TD configuration and residence times can be different. Particle loss in the

209   TD was characterized based on the single particle soot photometer (SP2) refractory black carbon

210   (rBC) mass measurement during the field campaign, since rBC does not evaporate even at 250°C.

211   The transmission efficiency of TD is about 90% (Fig. S3), similar to the values reported in previous

212   studies with similar TD configurations (Huffman et al., 2008; Massoli et al., 2015). The time scale

213   to reach thermodynamic equilibrium in a given TD depends on a number of factors, such as TD

214   temperature, aerosol mass concentration, aerosol diameter, and mass accommodation coefficient

215   (Riipinen et al., 2010; An et al., 2007; Saleh et al., 2011). In this study, we calculate the

216   characteristic time for aerosol equilibration by following the algorithm in Saleh et al. (2011). To

217   evaluate the equilibration time scale in the TD, the authors started with the mass transfer equation

218   (Eq. (1)) and then obtained the characteristic time for aerosol equilibration (τ in Eq. (2)) by

219   performing dimensional analysis.

220    $\dfrac{dC_a}{dt} = -2\pi d_p DFN_{tot}(KC_{g,sat} - C_g)$ Eq. (1)

221    $\tau = \dfrac{1}{2\pi d_p DFN_{tot}}$ Eq. (2)

222    $F = \dfrac{1+Kn}{1+0.3773Kn+1.33Kn(1+Kn)/\partial}$ Eq. (3)

223   In the equations, C_a, C_g, and $C_{g,sat}$ are the aerosol phase concentration, gas phase concentration, and

224   gas phase saturation concentration, respectively. N_{tot} is the total number concentration, d_p is the

225   particle size, D is the diffusion coefficient in the gas phase, K is the Kelvin effect correction, and

226   F is the Fuchs-Sutugin correction, which is calculated by Eq. (3). In Eq. (3), Kn is the Knudsen

227   number and α is the accommodation coefficient. D is on the order of 10^{-5} m^2 s^{-1} according to Tang

228   et al. (2015) and α is on the order of 0.1 as shown in Saleh et al. (2012). By using the campaign-

229   average particle number concentration (i.e., 4.28×10^3 cm^{-3}) and the mode of the particle number

230   distribution (i.e., 87nm) in our study, we estimate that the characteristic equilibration time is about

231   1600s, which is orders of magnitude longer than that residence time (5s) in the TD. Since the

232 evaporation process is likely far away from equilibrium, the gas phase saturation ratio is small and
233 the particles are likely evaporating in a vapor-free environment. Under this assumption, the gas
234 phase vapor concentration (i.e., C_g) in the mass transfer equation (Eq. (1)) can be neglected. After
235 integration over the residence time in the TD, the change in mass concentration upon heating (ΔC_a)
236 can be calculated by Eq. (4), in which $t_{residence}$ is the residence time in TD and the $\overline{C^*}$ is the
237 evaporation-time-averaged saturation concentration. Thus, the ΔC_a for each component is
238 proportional to its $\overline{C^*}$ because the other parameters are the same assuming the compounds are
239 internally mixed.

240 $$\Delta C_a = C_{t=0} - C_{t_{residence}} = \int_0^{t_{residence}} \frac{K C_{g,sat}}{\tau} dt = \frac{t_{residence}}{\tau} K \overline{C^*} \qquad \text{Eq. (4)}$$

241   A high-resolution time-of-flight aerosol mass spectrometer (HR-ToF-AMS, Aerodyne), a
242 soot-particle aerosol mass spectrometer (SP-AMS, Aerodyne), a single particle soot photometer
243 (SP2, DMT), and a scanning mobility particle sizer (SMPS, TSI) were placed downstream of the
244 TD. These four instruments alternated between sampling the bypass line (i.e., ambient) and the TD
245 line (i.e., thermally-denuded) every 10 min. When the instruments were sampling through the
246 bypass line, the heating section of TD was adjusted to the subsequent temperature setpoint. The
247 MFR was determined by comparing the measurements between bypass line and TD line.

248   The HR-ToF-AMS provides real-time measurements of the chemical composition and size
249 distribution of submicron non-refractory species (NR-PM$_1$) and has been described in detail
250 previously (Canagaratna et al., 2007; DeCarlo et al., 2006). In brief, the HR-ToF-AMS samples
251 particles through an aerodynamic lens and then impacts the focused particle beam on a heated
252 tungsten surface (~600°C). The resultant vapors are ionized by electron impact ionization and the
253 ions are analyzed using time-of-flight mass spectrometry. We used the ambient gas-phase CO_2
254 concentration (measured by a LI-COR CO_2 gas analyzer with 1 min resolution) to correct for the
255 gas-phase interference in the particle-phase CO_2^+ signals for both the bypass line and TD line. The
256 assumption behind this correction for the TD line is that the CO_2 generated in the TD, if it exists,
257 is negligible. Unless otherwise specified, the elemental ratios, such as atomic O:C and H:C, were
258 calculated based on the latest recommendation by Canagaratna et al. (2015), who modified the
259 original method developed for the HR-ToF-AMS (Aiken et al., 2007; Aiken et al., 2008). The HR-

260 ToF-AMS data were analyzed using the standard AMS analysis toolkits SQUIRREL v1.56A and
261 PIKA v1.15.

262   The SP-AMS measures the chemical composition of rBC containing particles by using an
263 intracavity laser vaporizer (1064 nm). The detailed working principles of SP-AMS are extensively
264 discussed in Onasch et al. (2012). In brief, after being focused through an aerodynamic lens, the
265 rBC-containing particles are heated and vaporized by laser absorption. The chemical composition
266 of both the rBC and any associated coatings are analyzed via high-resolution mass spectrometry.
267 The SP-AMS data presented in this paper were obtained between 5 and 15 February, 2012, when
268 the instrument was operated in the laser vaporizer only configuration, that is, only rBC-associated
269 species were detected. Analysis and interpretation of the SP-AMS measurements for the entire
270 deployment at Detling are presented in Williams et al. (2015).

271   The single particle soot photometer (SP2) measures rBC using laser-induced
272 incandescence. The method has been described previously (Schwarz et al., 2006; Stephens et al.,
273 2003). In brief, a 1064 nm Nd:YAG laser irradiates the particles as they enter the SP2, where upon
274 vaporization and incandescence is induced in the particles containing rBC. The incandescence
275 signal is proportional to the mass of rBC per particle, and with the sampling volume, rBC mass
276 concentrations are quantified. The SP2 at the Detling site was calibrated using fullerene soot (Alfa
277 Aesar, Inc., Ward Hill, Massachusetts; Stock# 40971, Lot# L18U002). Fullerene soot is an rBC
278 surrogate used for calibration of the SP2 due to its known density and similarities to ambient rBC
279 (Baumgardner et al., 2012; Laborde et al., 2012). Data analysis was performed with the Paul
280 Scherrer Institut Toolkit (PSI, Martin Gysel) developed for SP2 analysis within Igor Pro
281 (Wavemetrics, Inc.).

282 2.3 Collection efficiency of the HR-ToF-AMS

283   In order to provide quantitative data from HR-ToF-AMS measurements, the particle
284 collection efficiency (CE), which is largely due to particles bouncing on the vaporizer, needs to be
285 evaluated. For the bypass line, we calculated the CE based on the composition-dependent
286 algorithm proposed by Middlebrook et al. (2012) (i.e., CDCE). The CDCE for the bypass line
287 ranges from 0.45 to 0.97, with the campaign-averaged value 0.52 ± 0.08 (one standard deviation).
288 In order to validate the application of CDCE, we converted the mass concentrations of ambient

289 non-refractory species measured by HR-ToF-AMS (after CDCE correction) together with the mass

290 concentration of refractory species (i.e., rBC and crustal material) to volume using Eq. (5) and then

291 compared the calculated volume with SMPS measurements.

292 $\text{volume} = \dfrac{[NO_3^-]+[SO_4^{2-}]+[NH_4^+]}{1.75} + \dfrac{[Cl^-]}{1.52} + \dfrac{[\text{org}]}{\rho_{\text{org}}} + \dfrac{[\text{crustal material}]}{2.7} + \dfrac{[BC]}{0.73}$ Eq. (5)

293 In Eq. (5), 1.75 g cm^{-3} was used as the density for inorganic nitrate, sulfate, and ammonium,

294 and 1.52 g cm^{-3} was used as the density for chloride (Poulain et al., 2014). The density of ambient

295 organics was estimated using atomic O:C and H:C ratios as suggested by Kuwata et al. (2012). It

296 is noted that the O:C and H:C ratios calculated based on Aiken et al. (2008) were used in the

297 density estimation in order to be consistent with Kuwata et al. (2012). The organic density was

298 estimated to be 1.30, 1.42 and 1.68 g cm^{-3} for bypass line, TD = 120°C and TD = 250°C,

299 respectively. The estimated density values were within the literature range (Hallquist et al., 2009).

300 The concentration of crustal material was estimated by summing the normal oxides (Na$_2$O, MgO,

301 Al$_2$O$_3$, SiO$_2$, CaO, K$_2$O, FeO, Fe$_2$O$_3$, and TiO$_2$) of tracer elements (Malm et al., 1994). The tracer

302 elements were measured by PM$_{1.0-0.3}$ rotating drum impactors and analyzed by synchrotron

303 radiation-induced X-ray fluorescence spectrometry (Visser et al., 2015). The density of crustal

304 material (2.7 g cm^{-3}) was adapted from Lide (1991). The rBC concentration was measured by the

305 SP2. For the rBC density, many previous studies have used 1.77 g cm^{-3} (Salcedo et al., 2006;

306 Poulain et al., 2014; Huffman et al., 2009a). However, we note that 1.77 g cm^{-3} (adapted from Park

307 et al. (2004)) is the inherent material density of diesel soot particles. If the inherent material density

308 is used, one needs to consider the non-sphericity of rBC when comparing the calculated volume

309 to the SMPS volume as the particles are assumed to be spherical when estimating the SMPS

310 volume. In order to circumvent this issue, we used an effective density of rBC in this study. Park

311 et al. (2003) measured the effective density of diesel soot particles in the 50-300nm range (mobility

312 diameter) by using a Differential Mobility Analyzer - Aerosol Particle Mass analyzer (DMA -

313 APM) system. The soot particles were firstly classified based on mobility diameter in DMA and

314 the mass of classified particles was then measured by APM. The effective density was calculated

315 with the following equation by assuming spherical particles:

316
$$\rho_{eff} = \frac{mass}{\frac{\pi}{6} d_{me}^3}$$
Eq. (6)

317 where d_{me} is the mobility equivalent diameter. Thus, applying the effective density measured by a

318 DMA-APM system allows one to convert BC mass to its apparent volume, which is comparable

319 to the SMPS volume. One factor that complicates the choice of rBC effective density is that this

320 value decreases with increasing mobility diameter as shown in Park et al. (2003). Limited by the

321 lack of knowledge of the size distribution (mobility diameter based) of rBC in our data, we

322 calculated the average effective density based on all the values reported in Park et al. (2003) and

323 used this average value (0.73 g cm^{-3}) in our study. This simplification is reasonable considering

324 the following reasons. Firstly, Crilley et al. (2015) estimated that 70% of rBC at the Detling site is

325 from traffic, which is similar to the BC types in Park et al. (2003). Secondly, the size distribution

326 of total particles measured by SMPS in our study largely overlapped the size range studied in Park

327 et al. (2003).

328 The calculated volume (based on HR-ToF-AMS + rBC + crustal material) was then

329 compared with co-located SMPS measurements (Fig. 2). The SMPS measured the particle number

330 distribution between 15.1 and 532.8 nm mobility diameter. The number distribution can be

331 converted to a volume distribution assuming spherical particles. On average, the difference

332 between the calculated volume and the SMPS volume was within 6%, which validates the

333 application of CDCE for the bypass line (Fig. 2a).

334 However, the CDCE is not applicable for the TD line because the CDCE algorithm is

335 parameterized based on aerosol neutralization (Eq. (7)), which depends strongly on the accuracy

336 of the ammonium concentration measurement. The ammonium concentration decreased quickly

337 upon heating and was close to the instrument detection limit at 250°C. Thus, we evaluated the CE

338 for the TD line by comparing the calculated volume (based on HR-ToF-AMS + rBC + crustal

339 material) and the SMPS volume (Salcedo et al., 2006).

340
$$neutralization = \frac{NH_{4,meas}}{NH_{4,predict}} = \frac{NH_{4,meas}}{18 \times (\frac{SO_4 \times 2}{96} + \frac{NO_3}{62} + \frac{Chl}{35.5})}$$
Eq. (7)

341 We noted that the selection of the rBC density has a substantial effect on the TD line CE. For

342 example, varying the rBC density from 1.77 to 0.60 g cm^{-3} (i.e., from the inherent material density

343 to the effective density of 100 nm diesel soot particle reported in Park et al. (2003)) changed the

344 CE at 250°C by a factor of 2 (Table S1). This sensitivity analysis highlighted the importance of

345 the rBC density in applying this method to evaluate CE, especially for the TD line where rBC

346 accounted for a large fraction of the mass concentration. In this study, since the TD line CE

347 calculated with an rBC effective density of 0.73 g cm^{-3} (i.e., average value from Park et al. (2003))

348 was close to the default value for CE (i.e., 0.45), we used 0.45 as the TD line CE in our analysis.

349 As shown in Fig. 2b and 2c, the default CE results in a reasonable agreement between the

350 calculated volume and the SMPS volume for the TD line. Specifically, the differences between the

351 calculated volume and the SMPS volume are 14% and 11% at 120°C and 250°C, respectively,

352 which are within the range of measurement uncertainties. Future studies are warranted to

353 comprehensively investigate the change of AMS CE after heating of the aerosol.

354 2.3 Data analysis

355 2.3.1 Positive matrix factorization (PMF) analysis

356 Positive Matrix Factorization (PMF) analysis has been widely used for aerosol source

357 apportionment in the AMS community. This technique represents the observed data as a linear

358 combination of factors with constant mass spectra but varying concentrations across time in the

359 dataset (Paatero and Tapper, 1994; Paatero, 1997). Two solvers have been used for PMF analysis

360 of AMS data, PMF2 and the multilinear engine (ME-2). The PMF2 solver does not require a priori

361 information, which avoids some subjectivity. The ME-2 solver uses a priori information to reduce

362 rotational ambiguity among possible solutions (Canonaco et al., 2013; Paatero, 1999).

363 For the ambient OA measurements, we used the standard PMF2 solver, which does not

364 include any a priori information. This analysis is denoted as PMF$_{ambient}$ and was performed using

365 the PMF Evaluation Toolkit (PET) software developed by Ulbrich et al. (2009). The error matrix

366 was pre-treated based on the procedure in Ulbrich et al. (2009). m/z's with signal-to-noise ratio in

367 the range 0.2-2 were down weighted by a factor of 2, and m/z's with signal-to-noise ratio smaller

368 than 0.2 were removed. Also, the contributions of O^+, HO^+, H_2O^+, CO^+ and CO_2^+ were down

369 weighted to avoid excessive weighting of CO_2^+ and related fragments. Following the detailed

13

370   procedure listed in Zhang et al. (2011), the PMF solutions were evaluated by investigating the key
371   diagnostic plots (Fig. S4), mass spectral signatures, correlations with external tracers, and the
372   diurnal profiles. The rotational ambiguity of the optimal solution was examined by changing the
373   FPEAK parameter from -1 to 1. In our case, an FPEAK value of 0 (Q/Q_{exp} = 1.804) was selected
374   because the correlations between factors and external tracers were not improved for FPEAK values
375   that were different from 0. We resolved three factors from $PMF_{ambient}$, i.e., hydrocarbon-like OA
376   (HOA), solid fuel OA (SFOA), and oxygenated OA (OOA), which are discussed in section 3.1.
377   The choice of a three-factor solution is discussed in detail in the SI (Fig. S5).

378   For the TD line measurements, we first tried the PMF2 solver on the combined ambient
379   and thermally-denuded OA spectra (denoted as $PMF_{ambient+TD}$); this is the same approach applied
380   in Huffman et al. (2009a). However, in this study, we encountered several issues in $PMF_{ambient+TD}$
381   analysis. The first issue we encountered is the "mixing" behavior of OA factors. For example, in
382   the three-factor solution of $PMF_{ambient+TD}$, one factor has similar fragmentation patterns as HOA
383   from $PMF_{ambient}$, but this factor also has substantial signal at $C_2H_4O_2^+$ (*m/z* 60, often used as a
384   tracer marker for SFOA) (Fig. S6). In addition, another factor from $PMF_{ambient+TD}$ has similar time
385   series as SFOA from $PMF_{ambient}$, but has similar mass spectrum as OOA from $PMF_{ambient}$. The
386   second issue we encountered is that the mass loading of the OOA factor is occasionally higher in
387   the TD runs compared to the preceding and succeeding bypass runs (Fig. S7). The reason for this
388   behavior is not clear, but it is likely caused by the fact that only highly oxidized species remain
389   upon heating and the mass spectrum of the remaining OA becomes more similar to the oxidized
390   OA factors. Thus, PMF analysis might overestimate the concentrations of the oxidized OA factor.
391   Overall, the PMF analysis on the combined bypass and TD line measurements by using the PMF2
392   solver without a priori information could not clearly separate OA factors. This is likely caused by
393   the fact that including the thermally denuded data might distort the PMF results by introducing
394   additional time variation in the mass spectra as pointed out by Huffman et al. (2009a).

395   Considering the above issues associated with $PMF_{ambient+TD}$, we performed PMF analysis
396   using the ME-2 solver on the TD line measurements by applying the factor profiles determined
397   from $PMF_{ambient}$ as a priori information, in order to improve the separation of OA factor. Data
398   obtained at 120°C and 250°C were analyzed separately in order to account for the variability of
399   factor mass spectra at different temperatures. The analyses for 120°C and 250°C are denoted as

400   ME-2$_{120C}$ and ME-2$_{250C}$, respectively, and were performed using the toolkit Source Finder (SoFi

401   v4.8) (Canonaco et al., 2013). The error matrix was pre-treated in the same way as for PMF$_{ambient}$.

402   As recommended by Canonaco et al. (2013) and Crippa et al. (2014), secondary factors (i.e., OOA

403   factor) were unconstrained and primary factors (i.e., HOA and SFOA) were constrained with a

404   small a value (e.g., <0.1), which allows small variations of the resolved factors compared to the

405   anchor profile in order to account for differences in ambient sources and avoid a mixing situation.

406   We performed sensitivity tests and found that increasing the a value from 0 to 0.1 only reduced

407   the fitting "residual" (i.e., Q/Q_{exp}) by <1% and had negligible influence on the factor profiles and

408   factor concentrations (Figs. S8 and S9) for both ME-2$_{120C}$ and ME-2$_{250C}$. Therefore, considering

409   that 1) the small effect of the a value, and 2) the fact that the anchor profiles of HOA and SFOA

410   resolved from PMF$_{ambient}$ were clearly separated, we selected 0 as the a value, which fully

411   constrained the profile of HOA and SFOA. The mass spectra of thermally-denuded OOA at 120°C

412   and 250°C, which were not constrained in ME-2$_{120C}$ and ME-2$_{250C}$, change slightly compared to

413   the ambient OOA mass spectrum (Fig. S10). The most discernable changes occur at f_{CHO+} (i.e.,

414   fraction of organic signal at CHO$^+$), f_{C2H3O+} and f_{CO2+}, suggesting that the composition of OOA is

415   different at different denuding temperatures.

416   2.3.2 Retroplume analysis

417   Retroplume analysis was performed using the Numerical Atmospheric-Dispersion

418   Modelling Environment (NAME) dispersion model (Jones et al., 2007) to identify the origin of air

419   masses. The NAME model used the Unified Model reanalysis of meteorological data and

420   generated the surface level pathways of air masses arriving at the site after 1 day of transport (i.e.,

421   1-day footprints). The domain of influence of the NAME run was divided into a number of

422   geographical regions (i.e., Atlantic ocean, Benelux area, etc, shown in Fig. S11) as described in

423   Fleming et al. (2012). For each 3-hour period, the fraction of air masses arriving from each region

424   was calculated. According to Liu et al. (2013), for the time periods when the fraction of one region

425   is greater than the 40th percentile of that region's air masses fraction, that region is deemed to have

426   a strong influence on the sampling site. Regions can also be grouped into broader sectors. In this

427   study, we focused on two broader sectors, the easterly sector (North France and Benelux area) and

428   the westerly sector (Atlantic and Ireland). It is important to note that sometimes the sampling site

429   is influenced by more than one sector.

430   In the following discussion, we first investigate the PM_1 composition and OA source
431   apportionment at the Detling site (section 3.1). Then in section 3.2, we compare the measurements
432   at the rural Detling site with the urban NK site to investigate the spatial variability of aerosol in
433   the greater London area. Lastly, we examine the aerosol volatility based on measurements at the
434   Detling site (section 3.3).

435   **3 Results and Discussion**

436   3.1 Aerosol characterization at the Detling site

437   Figure 3a shows the time series of PM_1 composition measured by HR-ToF-AMS (i.e., non-
438   refractory species) and SP2 (i.e., rBC). The campaign-average PM_1 concentration is 14 ± 12 µg m$^-$
439   ^{3} (average $\pm$ one standard deviation). The chemical composition of PM_1 is dominated by nitrate
440   and organics, which on average accounts for 32% and 31% of total PM_1 mass, respectively. The
441   other components include sulfate (17%), ammonium (14%), rBC (4.3%), and chloride (2.2%).
442   Based on the fragmentation pattern of nitrate functionality in the AMS (i.e., NO^+/NO_2^+ ratio), one
443   can determine whether the nitrate is of organic or inorganic origin (Farmer et al., 2010; Boyd et
444   al., 2015; Fry et al., 2009; Xu et al., 2015b). At the Detling site, the measured NO^+/NO_2^+ ratio is
445   close to the value of pure ammonium nitrate (Fig. S12), indicating that the majority of the measured
446   nitrates are inorganic nitrates.

447   The PMF analysis on the ambient organic mass spectra (i.e., $PMF_{ambient}$) resolves three OA
448   subtypes: oxygenated organic aerosol (OOA), solid fuel organic aerosol (SFOA), and
449   hydrocarbon-like organic aerosol (HOA), which accounts for 54%, 23%, and 19% of total OA,
450   respectively. The time series and mass spectra of the three factors are shown in Fig. 4. HOA is
451   representative of primary OA from vehicle emissions as its mass spectrum is dominated by
452   hydrocarbon-like ions (i.e., $C_xH_y^+$ ions). HOA is correlated with rBC and NO_x (Fig. 4a). SFOA is
453   a surrogate for fresh OA from solid fuel combustion, including biomass burning (Young et al.,
454   2015b). The mass spectrum of SFOA is characterized by prominent signals at $C_2H_4O_2^+$ (m/z 60)
455   and $C_3H_5O_2^+$ (m/z 73), which are likely fragments from anhydrosugars such as levoglucosan and
456   mannosan (tracers for biomass burning). The time series of SFOA correlates with particle-phase
457   nitrated phenol compounds (Mohr et al., 2013), which are mainly associated with coal and wood
458   combustion (Fig. 4b). OOA is the most oxidized (O:C = 0.92) among all three factors. At the

459   Detling site, the OOA time series shows a good correlation with sulfate (Pearson's R=0.80, Fig.

460   4a) and acetaldehyde (R=0.78, Fig. 4a). Acetaldehyde could arise from direct emissions, such as

461   fossil fuel combustion and biomass burning, and secondary production by oxidation of various

462   hydrocarbons (Langford et al., 2009). The observation that acetaldehyde correlates better with

463   OOA than SFOA (R = 0.78 vs. 0.66) is consistent with previous studies which showed that

464   acetaldehyde is dominated by secondary production after hours of photochemical processing

465   (Hayes et al., 2013; Sommariva et al., 2011; de Gouw et al., 2005).

466   The identification of the sources of OOA is challenging because the mass spectrum of OA

467   from different sources becomes more similar and resembles that of OOA with increasing

468   photochemical aging (Ng et al., 2010; Jimenez et al., 2009). For the Detling data, we hypothesize

469   that OOA is mainly from aged biomass burning. Liu et al. (2015) combined the PMF results from

470   our study with radiocarbon analysis and estimated that 73-90% of carbon in the OOA factor was

471   non-fossil. Biogenic emissions and biomass burning are the major sources for non-fossil carbon.

472   The large fraction of non-fossil carbon indicates that the OOA measured at the Detling site largely

473   arises from aged biomass burning because the concentration of biogenic VOCs is low in winter

474   due to cold temperature and reduced photosynthesis. For example, Yin et al. (2015) showed that

475   the concentrations of isoprene SOA tracers (i.e., methyltetrols) and α-pinene SOA tracers (pinic

476   acid and pinonic acid) at the NK site during the winter IOP are only 0.5 ng m^{-3} and 2.3 ng m^{-3},

477   respectively, which are substantially lower than the concentrations measured at US and European

478   sites during warmer months. Both laboratory studies and ambient measurements have revealed

479   that the oxidation of biomass burning OA is a rapid process (Hennigan et al., 2011; May et al.,

480   2012; Bougiatioti et al., 2014; Zhao et al., 2015). During the oxidation process, the mass spectrum

481   of biomass burning OA could lose its characteristic signature (i.e., $C_2H_4O_2^+$ and $C_3H_5O_2^+$) and

482   becomes progressively similar to that of OOA (Grieshop et al., 2009a; Hennigan et al., 2011).

483   Thus, the aged biomass burning OA could be apportioned to the OOA by PMF analysis. With this,

484   it is possible that the biomass burning OA contributes a larger fraction of ambient OA in winter

485   than what previous field studies suggested, where this factor was typically identified based on the

486   presence of larger signals at $C_2H_4O_2^+$ (*m/z* 60) and $C_3H_5O_2^+$ (*m/z* 73) alone.

487   Figure 3b shows the aerosol composition when air masses come from the easterly sector

488   (i.e., mainland Europe) and the westerly sector (i.e., Atlantic Ocean). The concentration of PM$_1$ is

489   five times higher for the easterly sector compared to the westerly sector. This is consistent with

490   previous studies which showed that elevated pollution levels in the southern UK were often

491   associated with heavily polluted air masses transported from mainland Europe (Charron et al.,

492   2013; Morgan et al., 2010; Morgan et al., 2015; Putaud et al., 2004). Similar to the greater London

493   area, Beekmann et al. (2015) found that 70% of fine PM in the Paris megacity was also largely

494   influenced by regional contribution from mainland Europe. A large fraction of OA from mainland

495   Europe is highly oxidized organic aerosol (i.e., OOA). For example, while the concentrations of

496   HOA and SFOA only double when the source of air masses switches from the Atlantic Ocean to

497   mainland Europe, the OOA concentration increases from ~0.5 $\mu g\ m^{-3}$ to ~3 $\mu g\ m^{-3}$ (Fig. 3b). The

498   higher contribution of OOA to total OA is consistent with the total OA from mainland Europe

499   being more oxidized than that from the Atlantic Ocean. In Fig. 5, we compare the OA oxidation

500   level for different air masses in the f_{44} (i.e., fraction of organic signal at m/z 44) vs. f_{43} (i.e., fraction

501   of organic signal at m/z 43) plot (Ng et al., 2010). The OA for the easterly sector has a higher f_{44}

502   compared to the westerly sector, suggesting that the air masses advected from mainland Europe

503   have undergone a larger extent of photochemical processing.

504   3.2 Comparison between London and Detling

505   In this section, we compare the two simultaneous HR-ToF-AMS measurements at the rural

506   Detling site and the urban NK site. Only the sampling periods (hourly basis) when both instruments

507   were operative from 20 January to 8 February, 2012 are included in the comparison, so that the

508   concentrations reported in this section are different from those reported in section 3.1, where the

509   whole data set at the Detling site (from 20 January to 15 February, 2012) is used.

510   3.2.1 Non-refractory species and OA factors comparison

511   The comparison between the Detling and NK sites in terms of concentration and diurnal

512   variation of the five NR-PM$_1$ species is shown in Fig. 6 and Fig. S13, respectively. The

513   concentration of nitrate is substantially higher at the urban NK site (i.e., 5.6 $\mu g\ m^{-3}$) than the rural

514   Detling site (3.5 $\mu g\ m^{-3}$). This observation is consistent with McMeeking et al. (2012), who

515   performed airborne measurements in the urban London region and observed an enhancement of

516   nitrate concentration inside urban plumes. The elevated nitrate concentration (largely inorganic

517   nitrate) at the urban site suggests that nitrate has a strong local contribution, likely due to the fact

18

518   that nitrate formation occurs rapidly and its major sources (i.e., oxidation of NO_x) are much higher

519   over inner London (Shaw et al., 2015). The sulfate concentration is well correlated between two

520   sites (R = 0.82, Fig. 7), consistent with previous findings that sulfate has a strong regional

521   contribution in the greater London area (Harrison et al., 2012; Yin et al., 2010). However, the

522   sulfate concentration is about 60% higher at the rural Detling site than the urban NK site. The

523   comparison of sulfate concentration between the rural and urban site depends on the origin of air

524   masses. As shown in Fig. S14, the sulfate concentrations agree well between the two sites when

525   air masses come from Atlantic Ocean (i.e., westerly) compared to mainland Europe (i.e., easterly).

526   The reason for the elevated sulfate concentration at the rural site will be discussed below.

527   Although the average concentration of total OA is comparable between NK (i.e., 4.3 µg m^{-}

528   ^{3}) and Detling (4.0 µg m^{-3}) (Fig. 6), PMF analysis reveals that the contribution to total OA from

529   different sources is distinctly different between the urban and rural sites. At the urban NK site,

530   primary OA sources, including cooking, vehicle emission, and solid fuel combustion, account for

531   about 70% of total OA. At the rural Detling site, in contrast, more than half of the total OA is aged

532   secondary OA (i.e., OOA). Specifically, the cooking OA (i.e., COA), which accounts for 18% of

533   total OA at the urban NK site, is not resolved at the rural Detling site. This is expected as there is

534   no cooking activity near the rural Detling site. Hydrocarbon-like OA (i.e., HOA) only shows weak

535   correlation between the two sites (R = 0.53) (Fig. 8f), which is because HOA is representative of

536   primary OA and it is influenced by local vehicle emissions. The SFOA time series is moderately

537   correlated (R = 0.65) between Detling and NK (Fig. 8d). The SFOA concentration at the urban NK

538   site is almost twice as high at the rural Detling site, which is likely due to the elevated domestic

539   space heating activities and related emissions in the urban London area during wintertime (Young

540   et al., 2015b; Crilley et al., 2015).

541   Among all three OA factors, the OOA factor has the strongest correlation between the two

542   sites (R = 0.81) (Fig. 8b), which suggests that OOA likely represents regional SOA. Crilley et al.

543   (2015) also observed that the filter-based daily-average OC concentration is well correlated ($R^2 >$

544   0.82) between Detling and NK sites during the same period as our study. However, the good

545   correlations of OOA and OC observed in our study and Crilley et al. (2015) are different from the

546   observation in Charron et al. (2013), where the authors found that secondary organic carbon (SOC)

547   was much less spatially homogeneous than nitrate and sulfate by comparing an urban (Birmingham

548   site) and a rural site (Harwell site) in the greater London area between July and November 2010.

549   The difference between this study and Charron et al. (2013) is likely due to the uncertainty in the

550   SOC estimation method. In Charron et al. (2013), SOC is estimated from filter measured total OC

551   by using the EC/OC method where a constant EC/CC ratio from primary sources is applied. As

552   discussed in Charron et al. (2013), their estimation and the weak correlation of OC between

553   different sites are affected by the uncertainties associated with the choice of source ratios and

554   analytical procedure. In addition to SOC estimation uncertainty, the differences in sampling sites,

555   sampling periods, and size cuts ($PM_{2.5}$ vs. PM_1) between Charron et al. (2013) and our study could

556   also play a role.

557   Although the OOA is well-correlated between the two sites, the OOA concentration is

558   almost twice as high at the rural Detling site than the urban NK site (Fig. 6). This observation is

559   similar to the comparison of sulfate between the two sites, which is also usually considered to be

560   regional, as discussed above. Based on atmospheric chemistry transport model, the higher OOA

561   concentration at the rural site is a result of meteorological conditions, which cause a strong gradient

562   of SOA concentration when air masses are advected from polluted mainland Europe. For example,

563   to simulate the SOA formation in the winter IOP, Ots et al. (2015) applied the regional EMEP4UK

564   (European Monitoring and Evaluation Programme) model, which uses 5 km by 5 km British Isles

565   grid nested within 50 km by 50 km greater Europe domain, 21 vertical levels, Weather Research

566   and Forecasting (WRF) model meteorological reanalysis, and National Atmospheric Emissions

567   Inventory (NAEI) for the UK, Centre on Emission Inventories and Projections (CEIP) emissions

568   for other European countries. They observed a steep negative gradient of SOA concentration from

569   near European continent to southern England. The steep gradient is a result of meteorological

570   conditions (i.e., mainly wind direction), which causes that the pollution plume from mainland

571   Europe largely passes over the rural site, but not the urban site.

572   3.2.2 OA oxidation level

573   Figure 5 compares the OA oxidation level between Detling and NK. Compared to the NK

574   site, the average OA at the Detling site has higher f_{44}, indicating that the OA at the Detling site is

575   more oxidized than that at the NK site. The difference in OA oxidation level between the Detling

576   and the NK sites are due to different OA compositions. As shown in Fig. 6, the OA at the NK site

577   is dominated by primary OA (~70% of total OA) from cooking, vehicle emissions, and solid fuel

20

578   combustion, whose O:C is much lower than OOA. In contrast, more than half of OA at the Detling
579   site is OOA, which is highly oxidized.

580   3.3 Aerosol volatility analysis

581   3.3.1 Volatility of non-refractory species and OA factors

582   Figure 9a and c show the thermograms and the change in concentration after heating (ΔC)
583   of non-refractory (NR) species as measured by the HR-ToF-AMS. The MFR is calculated as the
584   ratio of the species mass concentration through the TD to the average mass concentration of the
585   preceding and succeeding bypass runs. The ΔC is calculated as the concentration difference
586   between the bypass and TD runs (Eq. (4)). Both the MFR and the ΔC have been corrected for the
587   particle loss in the thermal denuder (TD) by using the TD transmission efficiency as discussed in
588   section 2.2. The MFR of NR species is consistent with previous ambient measurements (Huffman
589   et al., 2009a). Nitrate has the largest average ΔC and the smallest MFR among all NR species. The
590   MFR of nitrate decreases to 0.15 at 120°C and it volatilizes completely at 250°C (i.e., MFR <
591   0.05). Sulfate is the least volatile species at 120°C, which has the smallest average ΔC and an MFR
592   equal to 0.89. The sulfate MFR is higher than that of ammonium sulfate from laboratory studies,
593   which has been attributed to particle mixing state affecting the sulfate volatility (Huffman et al.,
594   2009a; Massoli et al., 2015). For OA, the MFR is about 0.16 at 250°C. On average, 0.88 μg m^{-3}
595   OA remains after heating, implying the existence of non-volatile organic compounds. Figure 9d
596   shows that the ΔC's of three OA factors are not statistically different at 120°C. This suggests that
597   although the O:C of OOA (O:C = 0.92) is substantially larger than that of HOA (O:C = 0.22) and
598   SFOA (O:C = 0.37), the volatilities of the three factors are similar at 120°C. Thus, the O:C may
599   not be a good indicator of the volatility of the OA factors. At 250°C, both HOA and SFOA fully
600   evaporate (MFR < 0.05) so that the volatility cannot be compared under this temperature.

601   3.3.2 Sources of residual organics at 250°C

602   Figure 10 shows the chemical composition of the residual PM$_1$ after heating to 250°C. The
603   major components of the residual PM$_1$ are OA (90% of OA is OOA), rBC, and sulfate. rBC
604   accounts for about 30% of the remaining mass. This value is smaller than that reported in Poulain
605   et al. (2014) (i.e., 47% in summer and 59% in winter for TD temperature 300°C) and in Häkkinen
606   et al. (2012) (i.e., 55-87% depending on season for TD temperature 280°C). The differences are

607 likely due to 1) the density of rBC used in previous studies when converting SMPS volume
608 concentration to mass concentration, 2) different TD temperatures and residence times, 3)
609 techniques to measure rBC concentration, and 4) sampling locations.

610 At 250°C, OA has the largest contribution (~40%) to the residual mass. The existence of
611 highly oxidized, non-volatile organic compounds is consistent with previous ambient
612 measurements and model studies. For example, Cappa and Jimenez (2010) used a kinetic model
613 to simulate the volatility of OA factors measured by Huffman et al. (2009a) in the MILAGRO
614 field campaign and the authors estimated that a large fraction of OA was non-volatile and would
615 not evaporate under any atmospheric conditions.

616 The sources of non-volatile organics are uncertain, but appear to be related to
617 anthropogenic emissions. A previous study by Häkkinen et al. (2012) showed that the MFR
618 (excluding rBC) at 280°C correlated well with anthropogenic tracers (i.e., polycyclic aromatic
619 hydrocarbons), indicating that the non-volatile species may be affected by anthropogenic
620 emissions. In this study, we investigate the sources of the non-volatile organics by comparing the
621 measurements of HR-ToF-AMS and SP-AMS after heating at 250°C. While the HR-ToF-AMS
622 measures the bulk total non-refractory organics, SP-AMS only detects the organics associated with
623 rBC when the SP-AMS is operated with the laser vaporizer only (i.e., no tungsten vaporizer)
624 (Onasch et al., 2012). Figure 11 shows that after heating at 250°C, the residual organics associated
625 with rBC correlate well with the residual organics in the bulk measurements, and they only account
626 for <10% of the bulk measurements. Therefore, this good correlation is not caused by a large
627 contribution from rBC-associated species, but is possibly caused by the fact that the non-volatile
628 organics in the bulk measurements have similar sources or have undergone similar chemical
629 processing as rBC in the atmosphere. Denkenberger et al. (2007) suggested that the non-volatile
630 organics may be oligomers formed within the TD based on the observation that oligomer intensity
631 increased after heating ambient particles in a TD. In our study, the signals at high m/z (100 – 180),
632 which are potential indicators for oligomers, decrease with TD temperature (Fig. S15). This
633 suggests that the non-volatile organics are unlikely to be oligomers formed within the TD.

3.3.3 OA MFR and O:C ratio

To examine the relationship between O:C and MFR, the O:C of thermally-denuded OA is plotted as a function of TD temperature. As shown in Fig. 12a, the O:C of thermally-denuded OA increases with increasing TD temperature, indicating that the residual OA with lower volatility is more oxidized, which is consistent with previous observations (Huffman et al., 2009a; Huffman et al., 2009b). Thus, it appears that the OA oxidation level (i.e., O:C) is correlated with MFR. If so, one would expect that ambient OA with higher O:C should have larger MFR. However, as shown in Fig. 12b to e, the MFR increases only slightly with the bypass O:C (or OS) over a wide range of O:C (or OS). In addition, the correlation between MFR and bypass O:C (or OS) is weak (i.e., R < 0.4), suggesting that the volatility of OA cannot be readily inferred by its O:C or OS.

The lack of correlation between OA MFR and O:C is likely due to the distributions of volatility and O:C in bulk OA, that is, one population of particles with a higher bulk O:C could have lower MFR after heating compared to another population of particles with a lower bulk O:C, if the volatility and O:C distributions are different between two populations. In the following discussion, we use a simple model to illustrate our point (Fig. 13). Two populations of particles are comprised of three compounds (i.e., A, B, and C), but with different amounts. These three compounds have the same molecular weight, but different volatility and O:C. The assumed properties of the three compounds and the compositions of two populations of particles are atmospherically relevant and are summarized in Fig. 13. Although the average O:C of population #2 (i.e., 0.75) is higher than that of population #1 (i.e., 0.61), population #2 has the same MFR as population #1 after heating, which is consistent with the trend in Fig. 12b-e. On the other hand, the O:C of each population always increases after heating, which is consistent with the observation in Fig. 12a. We note that the example described here is specific; however, it clearly illustrates that the distributions of volatility and O:C largely influence the relationship between O:C and MFR of bulk OA. This also helps to explain the various types of relationship between O:C and MFR observed in laboratory studies (Grieshop et al., 2009b; Qi et al., 2010; Donahue et al., 2012; Kroll et al., 2009; Tritscher et al., 2011; Xu et al., 2014). In previous laboratory studies, while the SOA generally becomes progressively more oxidized (i.e., O:C increases) during the chemical aging, the volatility distribution evolves differently for different SOA systems, which results in various types of MFR trend (i.e., increases, or stays constant, or decreases over time). Our analysis

23

664 emphasizes the importance of understanding the distribution of volatility and O:C in bulk OA and
665 reveals the potential weakness of using one averaged O:C value to describe the degree of oxidation,
666 which is in line with the two-dimensional volatility-oxidation modeling framework proposed by
667 Donahue et al. (2011). In addition to the distribution of O:C and volatility, the fact that MFR
668 depends on the initial concentration of OA, which is different between studies, may also contribute
669 to the various relationships between O:C and MFR.

670 Hildebrandt et al. (2010) proposed that the lack of correlation between O:C and volatility
671 in Finokalia, Greece was caused by the OA being highly oxidized with an average O:C of 0.8
672 (estimated from the measured f_{44}). In order to test this hypothesis, we plot the O:C enhancement
673 (i.e., ratio between O:C of thermally denuded OA and O:C of ambient OA) vs. O:C of ambient
674 OA (Fig. 14a) to show the O:C enhancement after heating. By extrapolating the linear fit under
675 different temperatures, we find that if the O:C of ambient OA is about 1, the enhancement is
676 negligible even after heating at 250°C. It is important to note that the O:C reported in Fig. 14a is
677 calculated based on the recent formulation in Canagaratna et al. (2015). The improved O:C
678 calculation method in Canagaratna et al. (2015) results in higher O:C compared to the values based
679 on Aiken et al. (2008), which was used in Hildebrandt et al. (2010). By using the method in Aiken
680 et al. (2008), we found that the O:C threshold for no enhancement is 0.8 (Fig. S16), which is the
681 same as the O:C of ambient OA in Hildebrandt et al. (2010). In addition, the campaign-average f_{44}
682 of ambient OA in Hildebrandt et al. (2010) is 0.182, which is close to f_{44} of TD OA under 250°C
683 (i.e., 0.188) in our study (Fig. 14b). To conclude, this analysis provides a specific case in which
684 the average O:C ratio might not be a good indicator of OA volatility.

685 **4 Conclusions**

686 In this study, we deployed a suite of instruments to characterize the composition of PM_1 at
687 a rural site (Detling, Kent) near London during the Clean Air for London (ClearfLo) project in
688 2012 winter. Nitrate and organics are two major components in PM_1, each of which accounts for
689 ~30% of total PM_1 mass concentration. Retroplume analysis reveals that the PM_1 concentration in
690 the greater London area is largely influenced by the origin of the air masses. When air masses are
691 advected from mainland Europe, the PM_1 concentration is elevated and the organic aerosol is more
692 oxidized. Oxygenated organic aerosol (OOA) accounts for ~50% of total OA. Taking advantage

693   of measurements in winter when the biogenic emissions are low, we hypothesize that the OOA in

694   the current study is likely aged OA from biomass burning. The hypothesis is based on the

695   combined PMF and radiocarbon analysis where more than 70% of carbon in OOA is estimated to

696   be non-fossil (Liu et al., 2015) and cannot be explained by the small amount of biogenic SOA in

697   winter.

698   With simultaneous HR-ToF-AMS measurements taking place at the rural Detling site and

699   the urban North Kensington site, we have a unique opportunity to investigate the spatial variability

700   of PM_1 in the greater London area. The nitrate concentration is markedly higher at the urban site

701   compared to the rural site (i.e., 5.6 vs 3.5 μg m^{-3}). The high nitrate concentration at the rural site

702   together with the urban excess of nitrate imply that the nitrate in the greater London area has a

703   high regional background overlaid by important contributions from local production. Although the

704   OA concentration is comparable between the rural and urban sites, PMF analysis suggests

705   distinctly different contribution from different sources between the two sites. Similar to previous

706   studies, we find that OA at the urban site mainly arises from primary sources, while OA at the

707   rural site is mainly secondary. Vehicle emission, solid fuel combustion, and cooking together

708   account for ~70% of OA at the urban NK site. In contrast, OOA contributes more than half of total

709   OA at the rural Detling site. Among all OA factors, OOA has the best correlation between the two

710   sites (R = 0.81), which suggests that this factor is largely regional. We find that the OOA

711   concentration is almost twice as high at the rural Detling site than the urban NK site. This is a

712   result of meteorological conditions, which cause a strong gradient of SOA concentration when air

713   masses are advected from polluted mainland Europe. The observation that the OOA concentration

714   is higher at the rural site than urban site is opposite to the trend shown in Zhang et al. (2007).

715   However, the trend reported in Zhang et al. (2007) is not based on simultaneous measurements at

716   paired rural and urban sites. Thus, our observation highlights the importance of meteorology in

717   determining the OA spatial distribution.

718   A TD was deployed to investigate the volatility of PM_1 species at the Detling site. We find

719   that although OOA has substantial larger O:C than HOA and SFOA, the volatilities of these three

720   factors are similar at 120°C, which is inferred from the change in mass concentration after heating

721   at 120°C. This suggests that the O:C may not be a good proxy of OA factor volatility. We note

722   that 16% of total OA remains even after heating at 250°C, suggesting the existence of non-volatile

723 organics. PMF analysis reveals that the majority of the remaining organics are oxygenated OA. At
724 250°C, the time series of the residual organics measured by HR-ToF-AMS correlate well with the
725 residual organics associated with rBC measured by SP-AMS. The good correlation suggests that
726 the non-volatile organics likely have similar sources or have undergone similar chemical
727 processing as rBC in the atmosphere, considering that rBC-associated organics only account for
728 <10% of bulk organics.

729   We evaluate the relationship between the volatility (using the MFR) and degree of
730 oxidation (using the O:C or OS) of bulk OA. We found that, on the one hand, the O:C of thermally
731 denuded OA is higher than that of ambient OA, indicating that less-volatile compounds have
732 higher O:C. On the other hand, the MFR of OA shows a weak correlation with O:C of ambient
733 OA, indicating that the average O:C of bulk OA may not be a good indicator for volatility. One
734 possible explanation for the seemingly contradictory observations lies in the broad distribution of
735 volatility and O:C in bulk OA. For example, different O:C distributions could result in the same
736 bulk O:C but different volatility distributions, which may cause that particles with the same O:C
737 to have different MFR. Thus, it is important to understand and use the distribution of properties
738 (i.e., volatility and O:C) to describe the complexity of OA.

752 College London) and Roger Moore (Kent County Showgrounds) for assistance with the

753 organization of the field site in Detling, UK. Processed and quality assured data are available

754 through the ClearfLo project archive at the British Atmospheric Data Centre

755 (http://badc.nerc.ac.uk/browse/badc/clearflo) and through the US Department of Energy

756 Atmospheric Radiation Measurement Archive (www.archive.arm.gov). Raw data are archived at

757 the Georgia Institute of Technology and at Aerodyne Research, Inc. and are available on request.

758 **References**

759

760 Aiken, A. C., DeCarlo, P. F., and Jimenez, J. L.: Elemental Analysis of Organic Species with
761 Electron Ionization High-Resolution Mass Spectrometry, Anal Chem, 79, 8350-8358,
762 10.1021/ac071150w, 2007.

763

764 Aiken, A. C., Decarlo, P. F., Kroll, J. H., Worsnop, D. R., Huffman, J. A., Docherty, K. S., Ulbrich,
765 I. M., Mohr, C., Kimmel, J. R., Sueper, D., Sun, Y., Zhang, Q., Trimborn, A., Northway, M.,
766 Ziemann, P. J., Canagaratna, M. R., Onasch, T. B., Alfarra, M. R., Prevot, A. S. H., Dommen, J.,
767 Duplissy, J., Metzger, A., Baltensperger, U., and Jimenez, J. L.: O/C and OM/OC ratios of primary,
768 secondary, and ambient organic aerosols with high-resolution time-of-flight aerosol mass
769 spectrometry, Environ Sci Technol, 42, 4478-4485, Doi 10.1021/Es703009q, 2008.

770

771 An, W. J., Pathak, R. K., Lee, B. H., and Pandis, S. N.: Aerosol volatility measurement using an
772 improved thermodenuder: Application to secondary organic aerosol, J Aerosol Sci, 38, 305-314,
773 DOI 10.1016/j.jaerosci.2006.12.002, 2007.

774

775 Baumgardner, D., Popovicheva, O., Allan, J., Bernardoni, V., Cao, J., Cavalli, F., Cozic, J.,
776 Diapouli, E., Eleftheriadis, K., Genberg, P. J., Gonzalez, C., Gysel, M., John, A., Kirchstetter, T.
777 W., Kuhlbusch, T. A. J., Laborde, M., Lack, D., Muller, T., Niessner, R., Petzold, A., Piazzalunga,
778 A., Putaud, J. P., Schwarz, J., Sheridan, P., Subramanian, R., Swietlicki, E., Valli, G., Vecchi, R.,
779 and Viana, M.: Soot reference materials for instrument calibration and intercomparisons: a
780 workshop summary with recommendations, Atmos Meas Tech, 5, 1869-1887, DOI 10.5194/amt-
781 5-1869-2012, 2012.

782

783 Beekmann, M., Prévôt, A. S. H., Drewnick, F., Sciare, J., Pandis, S. N., Denier van der Gon, H. A.
784 C., Crippa, M., Freutel, F., Poulain, L., Ghersi, V., Rodriguez, E., Beirle, S., Zotter, P., von der
785 Weiden-Reinmüller, S. L., Bressi, M., Fountoukis, C., Petetin, H., Szidat, S., Schneider, J., Rosso,
786 A., El Haddad, I., Megaritis, A., Zhang, Q. J., Michoud, V., Slowik, J. G., Moukhtar, S., Kolmonen,
787 P., Stohl, A., Eckhardt, S., Borbon, A., Gros, V., Marchand, N., Jaffrezo, J. L., Schwarzenboeck,
788 A., Colomb, A., Wiedensohler, A., Borrmann, S., Lawrence, M., Baklanov, A., and Baltensperger,
789 U.: In situ, satellite measurement and model evidence on the dominant regional contribution to

790 fine particulate matter levels in the Paris megacity, Atmos. Chem. Phys., 15, 9577-9591,
791 10.5194/acp-15-9577-2015, 2015.
792

793 Bohnenstengel, S. I., Belcher, S. E., Aiken, A., Allan, J. D., Allen, G., Bacak, A., Bannan, T. J.,
794 Barlow, J. F., Beddows, D. C. S., Bloss, W. J., Booth, A. M., Chemel, C., Coceal, O., Di Marco,
795 C. F., Dubey, M. K., Faloon, K. H., Fleming, Z. L., Furger, M., Gietl, J. K., Graves, R. R., Green,
796 D. C., Grimmond, C. S. B., Halios, C. H., Hamilton, J. F., Harrison, R. M., Heal, M. R., Heard, D.
797 E., Helfter, C., Herndon, S. C., Holmes, R. E., Hopkins, J. R., Jones, A. M., Kelly, F. J., Kotthaus,
798 S., Langford, B., Lee, J. D., Leigh, R. J., Lewis, A. C., Lidster, R. T., Lopez-Hilfiker, F. D.,
799 McQuaid, J. B., Mohr, C., Monks, P. S., Nemitz, E., Ng, N. L., Percival, C. J., Prévôt, A. S. H.,
800 Ricketts, H. M. A., Sokhi, R., Stone, D., Thornton, J. A., Tremper, A. H., Valach, A. C., Visser,
801 S., Whalley, L. K., Williams, L. R., Xu, L., Young, D. E., and Zotter, P.: Meteorology, Air Quality,
802 and Health in London: The ClearfLo Project, B Am Meteorol Soc, 96, 779-804, 10.1175/BAMS-
803 D-12-00245.1, 2014.
804

805 Bougiatioti, A., Stavroulas, I., Kostenidou, E., Zarmpas, P., Theodosi, C., Kouvarakis, G.,
806 Canonaco, F., Prévôt, A. S. H., Nenes, A., Pandis, S. N., and Mihalopoulos, N.: Processing of
807 biomass-burning aerosol in the eastern Mediterranean during summertime, Atmos. Chem. Phys.,
808 14, 4793-4807, 10.5194/acp-14-4793-2014, 2014.
809

810 Boyd, C. M., Sanchez, J., Xu, L., Eugene, A. J., Nah, T., Tuet, W. Y., Guzman, M. I., and Ng, N.
811 L.: Secondary Organic Aerosol (SOA) formation from the β-pinene + NO3 system: effect of
812 humidity and peroxy radical fate, Atmos. Chem. Phys. Discuss., 15, 2679-2744, 10.5194/acpd-15-
813 2679-2015, 2015.
814

815 Canagaratna, M. R., Jayne, J. T., Jimenez, J. L., Allan, J. D., Alfarra, M. R., Zhang, Q., Onasch,
816 T. B., Drewnick, F., Coe, H., Middlebrook, A., Delia, A., Williams, L. R., Trimborn, A. M.,
817 Northway, M. J., DeCarlo, P. F., Kolb, C. E., Davidovits, P., and Worsnop, D. R.: Chemical and
818 microphysical characterization of ambient aerosols with the aerodyne aerosol mass spectrometer,
819 Mass Spectrometry Reviews, 26, 185-222, 10.1002/mas.20115, 2007.
820

821 Canagaratna, M. R., Jimenez, J. L., Kroll, J. H., Chen, Q., Kessler, S. H., Massoli, P., Hildebrandt
822 Ruiz, L., Fortner, E., Williams, L. R., Wilson, K. R., Surratt, J. D., Donahue, N. M., Jayne, J. T.,
823 and Worsnop, D. R.: Elemental ratio measurements of organic compounds using aerosol mass
824 spectrometry: characterization, improved calibration, and implications, Atmos. Chem. Phys., 15,
825 253-272, 10.5194/acp-15-253-2015, 2015.
826

827 Canonaco, F., Crippa, M., Slowik, J. G., Baltensperger, U., and Prévôt, A. S. H.: SoFi, an IGOR-
828 based interface for the efficient use of the generalized multilinear engine (ME-2) for the source
829 apportionment: ME-2 application to aerosol mass spectrometer data, Atmos. Meas. Tech., 6, 3649-
830 3661, 10.5194/amt-6-3649-2013, 2013.
831

832   Cappa, C. D., and Jimenez, J. L.: Quantitative estimates of the volatility of ambient organic aerosol,
833   Atmos. Chem. Phys., 10, 5409-5424, 10.5194/acp-10-5409-2010, 2010.
834

835   Charron, A., Degrendele, C., Laongsri, B., and Harrison, R. M.: Receptor modelling of secondary
836   and carbonaceous particulate matter at a southern UK site, Atmos. Chem. Phys., 13, 1879-1894,
837   10.5194/acp-13-1879-2013, 2013.
838

839   Crilley, L. R., Bloss, W. J., Yin, J., Beddows, D. C. S., Harrison, R. M., Allan, J. D., Young, D.
840   E., Flynn, M., Williams, P., Zotter, P., Prevot, A. S. H., Heal, M. R., Barlow, J. F., Halios, C. H.,
841   Lee, J. D., Szidat, S., and Mohr, C.: Sources and contributions of wood smoke during winter in
842   London: assessing local and regional influences, Atmos. Chem. Phys., 15, 3149-3171,
843   10.5194/acp-15-3149-2015, 2015.
844

845   Crippa, M., DeCarlo, P. F., Slowik, J. G., Mohr, C., Heringa, M. F., Chirico, R., Poulain, L., Freutel,
846   F., Sciare, J., Cozic, J., Di Marco, C. F., Elsasser, M., Nicolas, J. B., Marchand, N., Abidi, E.,
847   Wiedensohler, A., Drewnick, F., Schneider, J., Borrmann, S., Nemitz, E., Zimmermann, R.,
848   Jaffrezo, J. L., Prévôt, A. S. H., and Baltensperger, U.: Wintertime aerosol chemical composition
849   and source apportionment of the organic fraction in the metropolitan area of Paris, Atmos. Chem.
850   Phys., 13, 961-981, 10.5194/acp-13-961-2013, 2013.
851

852   Crippa, M., Canonaco, F., Lanz, V. A., Äijälä, M., Allan, J. D., Carbone, S., Capes, G., Ceburnis,
853   D., Dall'Osto, M., Day, D. A., DeCarlo, P. F., Ehn, M., Eriksson, A., Freney, E., Hildebrandt Ruiz,
854   L., Hillamo, R., Jimenez, J. L., Junninen, H., Kiendler-Scharr, A., Kortelainen, A. M., Kulmala,
855   M., Laaksonen, A., Mensah, A. A., Mohr, C., Nemitz, E., O'Dowd, C., Ovadnevaite, J., Pandis, S.
856   N., Petäjä, T., Poulain, L., Saarikoski, S., Sellegri, K., Swietlicki, E., Tiitta, P., Worsnop, D. R.,
857   Baltensperger, U., and Prévôt, A. S. H.: Organic aerosol components derived from 25 AMS data
858   sets across Europe using a consistent ME-2 based source apportionment approach, Atmos. Chem.
859   Phys., 14, 6159-6176, 10.5194/acp-14-6159-2014, 2014.
860

861   de Gouw, J. A., Middlebrook, A. M., Warneke, C., Goldan, P. D., Kuster, W. C., Roberts, J. M.,
862   Fehsenfeld, F. C., Worsnop, D. R., Canagaratna, M. R., Pszenny, A. A. P., Keene, W. C.,
863   Marchewka, M., Bertman, S. B., and Bates, T. S.: Budget of organic carbon in a polluted
864   atmosphere: Results from the New England Air Quality Study in 2002, J Geophys Res-Atmos,
865   110, Artn D16305 Doi 10.1029/2004jd005623, 2005.
866

867   DeCarlo, P. F., Kimmel, J. R., Trimborn, A., Northway, M. J., Jayne, J. T., Aiken, A. C., Gonin,
868   M., Fuhrer, K., Horvath, T., Docherty, K. S., Worsnop, D. R., and Jimenez, J. L.: Field-Deployable,
869   High-Resolution, Time-of-Flight Aerosol Mass Spectrometer, Anal Chem, 78, 8281-8289,
870   10.1021/ac061249n, 2006.
871

872 Denkenberger, K. A., Moffet, R. C., Holecek, J. C., Rebotier, T. P., and Prather, K. A.: Real-Time,
873 Single-Particle Measurements of Oligomers in Aged Ambient Aerosol Particles, Environ Sci
874 Technol, 41, 5439-5446, 10.1021/es070329l, 2007.
875

876 Donahue, N. M., Epstein, S. A., Pandis, S. N., and Robinson, A. L.: A two-dimensional volatility
877 basis set: 1. organic-aerosol mixing thermodynamics, Atmos. Chem. Phys., 11, 3303-3318,
878 10.5194/acp-11-3303-2011, 2011.
879

880 Donahue, N. M., Henry, K. M., Mentel, T. F., Kiendler-Scharr, A., Spindler, C., Bohn, B., Brauers,
881 T., Dorn, H. P., Fuchs, H., Tillmann, R., Wahner, A., Saathoff, H., Naumann, K. H., Mohler, O.,
882 Leisner, T., Muller, L., Reinnig, M. C., Hoffmann, T., Salo, K., Hallquist, M., Frosch, M., Bilde,
883 M., Tritscher, T., Barmet, P., Praplan, A. P., DeCarlo, P. F., Dommen, J., Prevot, A. S. H., and
884 Baltensperger, U.: Aging of biogenic secondary organic aerosol via gas-phase OH radical reactions,
885 P Natl Acad Sci USA, 109, 13503-13508, DOI 10.1073/pnas.1115186109, 2012.
886

887 Farmer, D. K., Matsunaga, A., Docherty, K. S., Surratt, J. D., Seinfeld, J. H., Ziemann, P. J., and
888 Jimenez, J. L.: Response of an aerosol mass spectrometer to organonitrates and organosulfates and
889 implications for atmospheric chemistry, Proceedings of the National Academy of Sciences, 107,
890 6670-6675, 10.1073/pnas.0912340107, 2010.
891

892 Fleming, Z. L., Monks, P. S., and Manning, A. J.: Review: Untangling the influence of air-mass
893 history in interpreting observed atmospheric composition, Atmos Res, 104–105, 1-39,
894 doi.org/10.1016/j.atmosres.2011.09.009, 2012.
895

896 Fry, J. L., Kiendler-Scharr, A., Rollins, A. W., Wooldridge, P. J., Brown, S. S., Fuchs, H., Dube,
897 W., Mensah, A., dal Maso, M., Tillmann, R., Dorn, H. P., Brauers, T., and Cohen, R. C.: Organic
898 nitrate and secondary organic aerosol yield from NO3 oxidation of beta-pinene evaluated using a
899 gas-phase kinetics/aerosol partitioning model, Atmos Chem Phys, 9, 1431-1449, 2009.
900

901 Grieshop, A. P., Donahue, N. M., and Robinson, A. L.: Laboratory investigation of photochemical
902 oxidation of organic aerosol from wood fires 2: analysis of aerosol mass spectrometer data, Atmos.
903 Chem. Phys., 9, 2227-2240, 10.5194/acp-9-2227-2009, 2009a.
904

905 Grieshop, A. P., Logue, J. M., Donahue, N. M., and Robinson, A. L.: Laboratory investigation of
906 photochemical oxidation of organic aerosol from wood fires 1: measurement and simulation of
907 organic aerosol evolution, Atmos. Chem. Phys., 9, 1263-1277, 10.5194/acp-9-1263-2009, 2009b.
908

909 Häkkinen, S. A. K., Äijälä, M., Lehtipalo, K., Junninen, H., Backman, J., Virkkula, A., Nieminen,
910 T., Vestenius, M., Hakola, H., Ehn, M., Worsnop, D. R., Kulmala, M., Petäjä, T., and Riipinen, I.:
911 Long-term volatility measurements of submicron atmospheric aerosol in Hyytiälä, Finland, Atmos.
912 Chem. Phys., 12, 10771-10786, 10.5194/acp-12-10771-2012, 2012.

913

914 Hallquist, M., Wenger, J. C., Baltensperger, U., Rudich, Y., Simpson, D., Claeys, M., Dommen,
915 J., Donahue, N. M., George, C., Goldstein, A. H., Hamilton, J. F., Herrmann, H., Hoffmann, T.,
916 Iinuma, Y., Jang, M., Jenkin, M. E., Jimenez, J. L., Kiendler-Scharr, A., Maenhaut, W., McFiggans,
917 G., Mentel, T. F., Monod, A., Prevot, A. S. H., Seinfeld, J. H., Surratt, J. D., Szmigielski, R., and
918 Wildt, J.: The formation, properties and impact of secondary organic aerosol: current and emerging
919 issues, Atmos Chem Phys, 9, 5155-5236, 2009.
920

921 Harrison, R. M., Dall'Osto, M., Beddows, D. C. S., Thorpe, A. J., Bloss, W. J., Allan, J. D., Coe,
922 H., Dorsey, J. R., Gallagher, M., Martin, C., Whitehead, J., Williams, P. I., Jones, R. L., Langridge,
923 J. M., Benton, A. K., Ball, S. M., Langford, B., Hewitt, C. N., Davison, B., Martin, D., Petersson,
924 K. F., Henshaw, S. J., White, I. R., Shallcross, D. E., Barlow, J. F., Dunbar, T., Davies, F., Nemitz,
925 E., Phillips, G. J., Helfter, C., Di Marco, C. F., and Smith, S.: Atmospheric chemistry and physics
926 in the atmosphere of a developed megacity (London): an overview of the REPARTEE experiment
927 and its conclusions, Atmos. Chem. Phys., 12, 3065-3114, 10.5194/acp-12-3065-2012, 2012.
928

929 Hayes, P. L., Ortega, A. M., Cubison, M. J., Froyd, K. D., Zhao, Y., Cliff, S. S., Hu, W. W.,
930 Toohey, D. W., Flynn, J. H., Lefer, B. L., Grossberg, N., Alvarez, S., Rappenglueck, B., Taylor, J.
931 W., Allan, J. D., Holloway, J. S., Gilman, J. B., Kuster, W. C., De Gouw, J. A., Massoli, P., Zhang,
932 X., Liu, J., Weber, R. J., Corrigan, A. L., Russell, L. M., Isaacman, G., Worton, D. R., Kreisberg,
933 N. M., Goldstein, A. H., Thalman, R., Waxman, E. M., Volkamer, R., Lin, Y. H., Surratt, J. D.,
934 Kleindienst, T. E., Offenberg, J. H., Dusanter, S., Griffith, S., Stevens, P. S., Brioude, J., Angevine,
935 W. M., and Jimenez, J. L.: Organic aerosol composition and sources in Pasadena, California,
936 during the 2010 CalNex campaign, J Geophys Res-Atmos, 118, 9233-9257, Doi
937 10.1002/Jgrd.50530, 2013.
938

939 Hennigan, C. J., Miracolo, M. A., Engelhart, G. J., May, A. A., Presto, A. A., Lee, T., Sullivan, A.
940 P., McMeeking, G. R., Coe, H., Wold, C. E., Hao, W. M., Gilman, J. B., Kuster, W. C., de Gouw,
941 J., Schichtel, B. A., Collett Jr, J. L., Kreidenweis, S. M., and Robinson, A. L.: Chemical and
942 physical transformations of organic aerosol from the photo-oxidation of open biomass burning
943 emissions in an environmental chamber, Atmos. Chem. Phys., 11, 7669-7686, 10.5194/acp-11-
944 7669-2011, 2011.
945

946 Hildebrandt, L., Engelhart, G. J., Mohr, C., Kostenidou, E., Lanz, V. A., Bougiatioti, A., DeCarlo,
947 P. F., Prevot, A. S. H., Baltensperger, U., Mihalopoulos, N., Donahue, N. M., and Pandis, S. N.:
948 Aged organic aerosol in the Eastern Mediterranean: the Finokalia Aerosol Measurement
949 Experiment-2008, Atmos Chem Phys, 10, 4167-4186, DOI 10.5194/acp-10-4167-2010, 2010.
950

951 Hildebrandt Ruiz, L., Paciga, A. L., Cerully, K., Nenes, A., Donahue, N. M., and Pandis, S. N.:
952 Aging of secondary organic aerosol from small aromatic VOCs: changes in chemical composition,
953 mass yield, volatility and hygroscopicity, Atmos. Chem. Phys. Discuss., 14, 31441-31481,
954 10.5194/acpd-14-31441-2014, 2014.

955

956   Huang, X. F., He, L. Y., Hu, M., Canagaratna, M. R., Sun, Y., Zhang, Q., Zhu, T., Xue, L., Zeng,
957   L. W., Liu, X. G., Zhang, Y. H., Jayne, J. T., Ng, N. L., and Worsnop, D. R.: Highly time-resolved
958   chemical characterization of atmospheric submicron particles during 2008 Beijing Olympic
959   Games using an Aerodyne High-Resolution Aerosol Mass Spectrometer, Atmos Chem Phys, 10,
960   8933-8945, DOI 10.5194/acp-10-8933-2010, 2010.
961

962   Huffman, J. A., Ziemann, P. J., Jayne, J. T., Worsnop, D. R., and Jimenez, J. L.: Development and
963   Characterization of a Fast-Stepping/Scanning Thermodenuder for Chemically-Resolved Aerosol
964   Volatility Measurements, Aerosol Sci Tech, 42, 395-407, 10.1080/02786820802104981, 2008.
965

966   Huffman, J. A., Docherty, K. S., Aiken, A. C., Cubison, M. J., Ulbrich, I. M., DeCarlo, P. F.,
967   Sueper, D., Jayne, J. T., Worsnop, D. R., Ziemann, P. J., and Jimenez, J. L.: Chemically-resolved
968   aerosol volatility measurements from two megacity field studies, Atmos Chem Phys, 9, 7161-7182,
969   2009a.
970

971   Huffman, J. A., Docherty, K. S., Mohr, C., Cubison, M. J., Ulbrich, I. M., Ziemann, P. J., Onasch,
972   T. B., and Jimenez, J. L.: Chemically-Resolved Volatility Measurements of Organic Aerosol from
973   Different Sources, Environ Sci Technol, 43, 5351-5357, 10.1021/es803539d, 2009b.
974

975   Jimenez, J. L., Canagaratna, M. R., Donahue, N. M., Prevot, A. S. H., Zhang, Q., Kroll, J. H.,
976   DeCarlo, P. F., Allan, J. D., Coe, H., Ng, N. L., Aiken, A. C., Docherty, K. S., Ulbrich, I. M.,
977   Grieshop, A. P., Robinson, A. L., Duplissy, J., Smith, J. D., Wilson, K. R., Lanz, V. A., Hueglin,
978   C., Sun, Y. L., Tian, J., Laaksonen, A., Raatikainen, T., Rautiainen, J., Vaattovaara, P., Ehn, M.,
979   Kulmala, M., Tomlinson, J. M., Collins, D. R., Cubison, M. J., Dunlea, E. J., Huffman, J. A.,
980   Onasch, T. B., Alfarra, M. R., Williams, P. I., Bower, K., Kondo, Y., Schneider, J., Drewnick, F.,
981   Borrmann, S., Weimer, S., Demerjian, K., Salcedo, D., Cottrell, L., Griffin, R., Takami, A.,
982   Miyoshi, T., Hatakeyama, S., Shimono, A., Sun, J. Y., Zhang, Y. M., Dzepina, K., Kimmel, J. R.,
983   Sueper, D., Jayne, J. T., Herndon, S. C., Trimborn, A. M., Williams, L. R., Wood, E. C.,
984   Middlebrook, A. M., Kolb, C. E., Baltensperger, U., and Worsnop, D. R.: Evolution of Organic
985   Aerosols in the Atmosphere, Science, 326, 1525-1529, DOI 10.1126/science.1180353, 2009.
986   Jones, A., Thomson, D., Hort, M., and Devenish, B.: The U.K. Met Office's Next-Generation
987   Atmospheric Dispersion Model, NAME III, in: Air Pollution Modeling and Its Application XVII,
988   edited by: Borrego, C., and Norman, A.-L., Springer US, 580-589, 2007.
989

990   Jonsson, A. M., Hallquist, M., and Saathoff, H.: Volatility of secondary organic aerosols from the
991   ozone initiated oxidation of alpha-pinene and limonene, J Aerosol Sci, 38, 843-852, DOI
992   10.1016/j.jaerosci.2007.06.008, 2007.
993

994   Kroll, J. H., Smith, J. D., Che, D. L., Kessler, S. H., Worsnop, D. R., and Wilson, K. R.:
995   Measurement of fragmentation and functionalization pathways in the heterogeneous oxidation of
996   oxidized organic aerosol, Phys Chem Chem Phys, 11, 8005-8014, Doi 10.1039/B905289e, 2009.
997

998   Kuwata, M., Zorn, S. R., and Martin, S. T.: Using Elemental Ratios to Predict the Density of
999   Organic Material Composed of Carbon, Hydrogen, and Oxygen, Environ Sci Technol, 46, 787-
1000 794, 10.1021/es202525q, 2012.
1001

1002 Laborde, M., Mertes, P., Zieger, P., Dommen, J., Baltensperger, U., and Gysel, M.: Sensitivity of
1003 the Single Particle Soot Photometer to different black carbon types, Atmos Meas Tech, 5, 1031-
1004 1043, DOI 10.5194/amt-5-1031-2012, 2012.
1005

1006 Langford, B., Davison, B., Nemitz, E., and Hewitt, C. N.: Mixing ratios and eddy covariance flux
1007 measurements of volatile organic compounds from an urban canopy (Manchester, UK), Atmos.
1008 Chem. Phys., 9, 1971-1987, 10.5194/acp-9-1971-2009, 2009.
1009

1010 Lanz, V. A., Alfarra, M. R., Baltensperger, U., Buchmann, B., Hueglin, C., and Prevot, A. S. H.:
1011 Source apportionment of submicron organic aerosols at an urban site by factor analytical modelling
1012 of aerosol mass spectra, Atmos Chem Phys, 7, 1503-1522, 2007.
1013

1014 Lee, B. H., Pierce, J. R., Engelhart, G. J., and Pandis, S. N.: Volatility of secondary organic aerosol
1015 from the ozonolysis of monoterpenes, Atmospheric Environment, 45, 2443-2452, DOI
1016 10.1016/j.atmosenv.2011.02.004, 2011.
1017

1018 Lide, D. R.: CRC Handbook of Chemistry and Physics, CRC Press Inc, 1991.
1019

1020 Liu, D., Allan, J., Whitehead, J., Young, D., Flynn, M., Coe, H., McFiggans, G., Fleming, Z. L.,
1021 and Bandy, B.: Ambient black carbon particle hygroscopic properties controlled by mixing state
1022 and composition, Atmos. Chem. Phys., 13, 2015-2029, 10.5194/acp-13-2015-2013, 2013.
1023

1024 Liu, S., Aiken, A. C., Gorkowski, K., Dubey, M. K., Cappa, C. D., Williams, L. R., Herndon, S.
1025 C., Massoli, P., Fortner, E. C., Chhabra, P. S., Brooks, W. A., Onasch, T. B., Jayne, J. T., Worsnop,
1026 D. R., China, S., Sharma, N., Mazzoleni, C., Xu, L., Ng, N. L., Liu, D., Allan, J. D., Lee, J. D.,
1027 Fleming, Z. L., Mohr, C., Zotter, P., Szidat, S., and Prevot, A. S. H.: Enhanced light absorption by
1028 mixed source black and brown carbon particles in UK winter, Nat Commun, 6,
1029 10.1038/ncomms9435, 2015.
1030

1031 Malm, W. C., Sisler, J. F., Huffman, D., Eldred, R. A., and Cahill, T. A.: Spatial and seasonal
1032 trends in particle concentration and optical extinction in the United States, Journal of Geophysical
1033 Research: Atmospheres, 99, 1347-1370, 10.1029/93JD02916, 1994.

1034

Massoli, P., Onasch, T. B., Cappa, C. D., Nuamaan, I., Hakala, J., Hayden, K., Li, S.-M., Sueper, D. T., Bates, T. S., Quinn, P. K., Jayne, J. T., and Worsnop, D. R.: Characterization of black carbon-containing particles from soot particle aerosol mass spectrometer measurements on the R/V Atlantis during CalNex 2010, Journal of Geophysical Research: Atmospheres, 120, 2575-2593, 10.1002/2014JD022834, 2015.

May, A. A., Saleh, R., Hennigan, C. J., Donahue, N. M., and Robinson, A. L.: Volatility of Organic Molecular Markers Used for Source Apportionment Analysis: Measurements and Implications for Atmospheric Lifetime, Environ Sci Technol, 46, 12435-12444, 10.1021/es302276t, 2012.

McMeeking, G. R., Bart, M., Chazette, P., Haywood, J. M., Hopkins, J. R., McQuaid, J. B., Morgan, W. T., Raut, J. C., Ryder, C. L., Savage, N., Turnbull, K., and Coe, H.: Airborne measurements of trace gases and aerosols over the London metropolitan region, Atmos. Chem. Phys., 12, 5163-5187, 10.5194/acp-12-5163-2012, 2012.

Middlebrook, A. M., Bahreini, R., Jimenez, J. L., and Canagaratna, M. R.: Evaluation of Composition-Dependent Collection Efficiencies for the Aerodyne Aerosol Mass Spectrometer using Field Data, Aerosol Sci Tech, 46, 258-271, Doi 10.1080/02786826.2011.620041, 2012.

Mohr, C., DeCarlo, P. F., Heringa, M. F., Chirico, R., Slowik, J. G., Richter, R., Reche, C., Alastuey, A., Querol, X., Seco, R., Peñuelas, J., Jiménez, J. L., Crippa, M., Zimmermann, R., Baltensperger, U., and Prévôt, A. S. H.: Identification and quantification of organic aerosol from cooking and other sources in Barcelona using aerosol mass spectrometer data, Atmos. Chem. Phys., 12, 1649-1665, 10.5194/acp-12-1649-2012, 2012.

Mohr, C., Lopez-Hilfiker, F. D., Zotter, P., Prévôt, A. S. H., Xu, L., Ng, N. L., Herndon, S. C., Williams, L. R., Franklin, J. P., Zahniser, M. S., Worsnop, D. R., Knighton, W. B., Aiken, A. C., Gorkowski, K. J., Dubey, M. K., Allan, J. D., and Thornton, J. A.: Contribution of Nitrated Phenols to Wood Burning Brown Carbon Light Absorption in Detling, United Kingdom during Winter Time, Environ Sci Technol, 47, 6316-6324, 10.1021/es400683v, 2013.

Morgan, W. T., Allan, J. D., Bower, K. N., Highwood, E. J., Liu, D., McMeeking, G. R., Northway, M. J., Williams, P. I., Krejci, R., and Coe, H.: Airborne measurements of the spatial distribution of aerosol chemical composition across Europe and evolution of the organic fraction, Atmos. Chem. Phys., 10, 4065-4083, 10.5194/acp-10-4065-2010, 2010.

Morgan, W. T., Ouyang, B., Allan, J. D., Aruffo, E., Di Carlo, P., Kennedy, O. J., Lowe, D., Flynn, M. J., Rosenberg, P. D., Williams, P. I., Jones, R., McFiggans, G. B., and Coe, H.: Influence of aerosol chemical composition on N2O5 uptake: airborne regional measurements in northwestern Europe, Atmos. Chem. Phys., 15, 973-990, 10.5194/acp-15-973-2015, 2015.

1075

1076 Ng, N. L., Canagaratna, M. R., Zhang, Q., Jimenez, J. L., Tian, J., Ulbrich, I. M., Kroll, J. H.,
1077 Docherty, K. S., Chhabra, P. S., Bahreini, R., Murphy, S. M., Seinfeld, J. H., Hildebrandt, L.,
1078 Donahue, N. M., DeCarlo, P. F., Lanz, V. A., Prevot, A. S. H., Dinar, E., Rudich, Y., and Worsnop,
1079 D. R.: Organic aerosol components observed in Northern Hemispheric datasets from Aerosol Mass
1080 Spectrometry, Atmos Chem Phys, 10, 4625-4641, DOI 10.5194/acp-10-4625-2010, 2010.
1081

1082 Onasch, T. B., Trimborn, A., Fortner, E. C., Jayne, J. T., Kok, G. L., Williams, L. R., Davidovits,
1083 P., and Worsnop, D. R.: Soot Particle Aerosol Mass Spectrometer: Development, Validation, and
1084 Initial Application, Aerosol Sci Tech, 46, 804-817, 10.1080/02786826.2012.663948, 2012.
1085

1086 Ots, R., Young, D. E., Vieno, M., Xu, L., Dunmore, R. E., Allan, J. D., Coe, H., Williams, L. R.,
1087 Herndon, S. C., Ng, N. L., Hamilton, J. F., Bergström, R., Marco, C. D., Nemitz, E., Mackenzie,
1088 I. A., Kuenen, J. J. P., Green, D. C., Reis, S., and Heal, M. R. H.: Simulating secondary organic
1089 aerosol from missing diesel-related intermediate-volatility organic compound emissions during the
1090 Clean Air for London (ClearfLo) campaign, Submitted to Atmos. Chem. Phys. , 2015.
1091

1092 Paatero, P., and Tapper, U.: Positive Matrix Factorization - a Nonnegative Factor Model with
1093 Optimal Utilization of Error-Estimates of Data Values, Environmetrics, 5, 111-126, DOI
1094 10.1002/env.3170050203, 1994.
1095

1096 Paatero, P.: A weighted non-negative least squares algorithm for three-way 'PARAFAC' factor
1097 analysis, Chemometr Intell Lab, 38, 223-242, Doi 10.1016/S0169-7439(97)00031-2, 1997.
1098

1099 Paatero, P.: The Multilinear Engine—A Table-Driven, Least Squares Program for Solving
1100 Multilinear Problems, Including the n-Way Parallel Factor Analysis Model, Journal of
1101 Computational and Graphical Statistics, 8, 854-888, 10.1080/10618600.1999.10474853, 1999.
1102

1103 Paciga, A., Karnezi, E., Kostenidou, E., Hildebrandt, L., Psichoudaki, M., Engelhart, G. J., Lee, B.
1104 H., Crippa, M., Prévôt, A. S. H., Baltensperger, U., and Pandis, S. N.: Volatility of organic aerosol
1105 and its components in the Megacity of Paris, Atmos. Chem. Phys. Discuss., 15, 22263-22289,
1106 10.5194/acpd-15-22263-2015, 2015.
1107

1108 Park, K., Cao, F., Kittelson, D. B., and McMurry, P. H.: Relationship between Particle Mass and
1109 Mobility for Diesel Exhaust Particles, Environ Sci Technol, 37, 577-583, 10.1021/es025960v,
1110 2003.
1111

1112 Park, K., Kittelson, D., Zachariah, M., and McMurry, P.: Measurement of Inherent Material
1113 Density of Nanoparticle Agglomerates, J Nanopart Res, 6, 267-272,
1114 10.1023/B:NANO.0000034657.71309.e6, 2004.

1115

Poulain, L., Birmili, W., Canonaco, F., Crippa, M., Wu, Z. J., Nordmann, S., Spindler, G., Prévôt, A. S. H., Wiedensohler, A., and Herrmann, H.: Chemical mass balance of 300 °C non-volatile particles at the tropospheric research site Melpitz, Germany, Atmos. Chem. Phys., 14, 10145-10162, 10.5194/acp-14-10145-2014, 2014.

Putaud, J.-P., Raes, F., Van Dingenen, R., Brüggemann, E., Facchini, M. C., Decesari, S., Fuzzi, S., Gehrig, R., Hüglin, C., Laj, P., Lorbeer, G., Maenhaut, W., Mihalopoulos, N., Müller, K., Querol, X., Rodriguez, S., Schneider, J., Spindler, G., Brink, H. t., Tørseth, K., and Wiedensohler, A.: A European aerosol phenomenology—2: chemical characteristics of particulate matter at kerbside, urban, rural and background sites in Europe, Atmospheric Environment, 38, 2579-2595, http://dx.doi.org/10.1016/j.atmosenv.2004.01.041, 2004.

Qi, L., Nakao, S., Malloy, Q., Warren, B., and Cocker, D. R.: Can secondary organic aerosol formed in an atmospheric simulation chamber continuously age?, Atmospheric Environment, 44, 2990-2996, DOI 10.1016/j.atmosenv.2010.05.020, 2010.

Riipinen, I., Pierce, J. R., Donahue, N. M., and Pandis, S. N.: Equilibration time scales of organic aerosol inside thermodenuders: Evaporation kinetics versus thermodynamics, Atmospheric Environment, 44, 597-607, http://dx.doi.org/10.1016/j.atmosenv.2009.11.022, 2010.

Salcedo, D., Onasch, T. B., Dzepina, K., Canagaratna, M. R., Zhang, Q., Huffman, J. A., DeCarlo, P. F., Jayne, J. T., Mortimer, P., Worsnop, D. R., Kolb, C. E., Johnson, K. S., Zuberi, B., Marr, L. C., Volkamer, R., Molina, L. T., Molina, M. J., Cardenas, B., Bernabé, R. M., Márquez, C., Gaffney, J. S., Marley, N. A., Laskin, A., Shutthanandan, V., Xie, Y., Brune, W., Lesher, R., Shirley, T., and Jimenez, J. L.: Characterization of ambient aerosols in Mexico City during the MCMA-2003 campaign with Aerosol Mass Spectrometry: results from the CENICA Supersite, Atmos. Chem. Phys., 6, 925-946, 10.5194/acp-6-925-2006, 2006.

Saleh, R., Shihadeh, A., and Khlystov, A.: On transport phenomena and equilibration time scales in thermodenuders, Atmos. Meas. Tech., 4, 571-581, 10.5194/amt-4-571-2011, 2011.

Saleh, R., Khlystov, A., and Shihadeh, A.: Determination of Evaporation Coefficients of Ambient and Laboratory-Generated Semivolatile Organic Aerosols from Phase Equilibration Kinetics in a Thermodenuder, Aerosol Sci Tech, 46, 22-30, 10.1080/02786826.2011.602762, 2012.

Schwarz, J. P., Gao, R. S., Fahey, D. W., Thomson, D. S., Watts, L. A., Wilson, J. C., Reeves, J. M., Darbeheshti, M., Baumgardner, D. G., Kok, G. L., Chung, S. H., Schulz, M., Hendricks, J., Lauer, A., Karcher, B., Slowik, J. G., Rosenlof, K. H., Thompson, T. L., Langford, A. O., Loewenstein, M., and Aikin, K. C.: Single-particle measurements of midlatitude black carbon and

1155 light-scattering aerosols from the boundary layer to the lower stratosphere, J Geophys Res-Atmos,
1156 111, Doi 10.1029/2006jd007076, 2006.
1157

1158 Shaw, M. D., Lee, J. D., Davison, B., Vaughan, A., Purvis, R. M., Harvey, A., Lewis, A. C., and
1159 Hewitt, C. N.: Airborne determination of the temporo-spatial distribution of benzene, toluene,
1160 nitrogen oxides and ozone in the boundary layer across Greater London, UK, Atmos. Chem. Phys.,
1161 15, 5083-5097, 10.5194/acp-15-5083-2015, 2015.
1162

1163 Sommariva, R., de Gouw, J. A., Trainer, M., Atlas, E., Goldan, P. D., Kuster, W. C., Warneke, C.,
1164 and Fehsenfeld, F. C.: Emissions and photochemistry of oxygenated VOCs in urban plumes in the
1165 Northeastern United States, Atmos. Chem. Phys., 11, 7081-7096, 10.5194/acp-11-7081-2011,
1166 2011.
1167

1168 Stanier, C. O., Pathak, R. K., and Pandis, S. N.: Measurements of the volatility of aerosols from
1169 alpha-piniene ozonolysis, Environ Sci Technol, 41, 2756-2763, Doi 10.1021/Es0519280, 2007.
1170

1171 Stephens, M., Turner, N., and Sandberg, J.: Particle identification by laser-induced incandescence
1172 in a solid-state laser cavity, Appl Optics, 42, 3726-3736, Doi 10.1364/Ao.42.003726, 2003.
1173

1174 Tang, M. J., Shiraiwa, M., Pöschl, U., Cox, R. A., and Kalberer, M.: Compilation and evaluation
1175 of gas phase diffusion coefficients of reactive trace gases in the atmosphere: Volume 2.
1176 Diffusivities of organic compounds, pressure-normalised mean free paths, and average Knudsen
1177 numbers for gas uptake calculations, Atmos. Chem. Phys., 15, 5585-5598, 10.5194/acp-15-5585-
1178 2015, 2015.
1179

1180 Tritscher, T., Dommen, J., DeCarlo, P. F., Gysel, M., Barmet, P. B., Praplan, A. P., Weingartner,
1181 E., Prévôt, A. S. H., Riipinen, I., Donahue, N. M., and Baltensperger, U.: Volatility and
1182 hygroscopicity of aging secondary organic aerosol in a smog chamber, Atmos. Chem. Phys., 11,
1183 11477-11496, 10.5194/acp-11-11477-2011, 2011.
1184

1185 Ulbrich, I. M., Canagaratna, M. R., Zhang, Q., Worsnop, D. R., and Jimenez, J. L.: Interpretation
1186 of organic components from Positive Matrix Factorization of aerosol mass spectrometric data,
1187 Atmos. Chem. Phys., 9, 2891-2918, 10.5194/acp-9-2891-2009, 2009.
1188

1189 Visser, S., Slowik, J. G., Furger, M., Zotter, P., Bukowiecki, N., Dressler, R., Flechsig, U., Appel,
1190 K., Green, D. C., Tremper, A. H., Young, D. E., Williams, P. I., Allan, J. D., Herndon, S. C.,
1191 Williams, L. R., Mohr, C., Xu, L., Ng, N. L., Detournay, A., Barlow, J. F., Halios, C. H., Fleming,
1192 Z. L., Baltensperger, U., and Prévôt, A. S. H.: Kerb and urban increment of highly time-resolved
1193 trace elements in PM10, PM2.5 and PM1.0 winter aerosol in London during ClearfLo 2012, Atmos.
1194 Chem. Phys., 15, 2367-2386, 10.5194/acp-15-2367-2015, 2015.
1195

1196 Williams, L., Herndon, S., Jayne, J., Freedman, A., Brooks, B., Franklin, J. P., Massoli, P., Fortner,
1197 E., Chhabra, P. S., Zahniser, M. S., Stark, H., canagaratna, M., Onasch, T., Worsnop, D., Ng, N.
1198 L., Xu, L., Knighton, B., Aiken, A., Gorkowski, K. J., Liu, S., Martin, A. T., Coulter, R., Lopez-
1199 Hilfiker, F. D., Mohr, C., Thornton, J., Visser, S., Furger, M., Zotter, P., and Prevot, A. S. H.:
1200 Characterization of black carbon containing particles in rural wintertime UK with an Aerodyne
1201 soot particle aerosol mass spectrometer (SP-AMS), Atmos. Chem. Phys. Discuss., in preparation,
1202 2015.
1203

1204 Xu, L., Kollman, M. S., Song, C., Shilling, J. E., and Ng, N. L.: Effects of NOx on the Volatility
1205 of Secondary Organic Aerosol from Isoprene Photooxidation, Environ Sci Technol, 48, 2253-2262,
1206 10.1021/es404842g, 2014.
1207

1208 Xu, L., Guo, H., Boyd, C. M., Klein, M., Bougiatioti, A., Cerully, K. M., Hite, J. R., Isaacman-
1209 VanWertz, G., Kreisberg, N. M., Knote, C., Olson, K., Koss, A., Goldstein, A. H., Hering, S. V.,
1210 de Gouw, J., Baumann, K., Lee, S.-H., Nenes, A., Weber, R. J., and Ng, N. L.: Effects of
1211 anthropogenic emissions on aerosol formation from isoprene and monoterpenes in the southeastern
1212 United States, Proceedings of the National Academy of Sciences, 112, 37-42,
1213 10.1073/pnas.1417609112, 2015a.
1214

1215 Xu, L., Suresh, S., Guo, H., Weber, R. J., and Ng, N. L.: Aerosol characterization over the
1216 southeastern United States using high resolution aerosol mass spectrometry: spatial and seasonal
1217 variation of aerosol composition, sources, and organic nitrates, Atmos. Chem. Phys. Discuss., 15,
1218 10479-10552, 10.5194/acpd-15-10479-2015, 2015b.
1219

1220 Yin, J., Harrison, R. M., Chen, Q., Rutter, A., and Schauer, J. J.: Source apportionment of fine
1221 particles at urban background and rural sites in the UK atmosphere, Atmospheric Environment,
1222 44, 841-851, http://dx.doi.org/10.1016/j.atmosenv.2009.11.026, 2010.
1223

1224 Yin, J., Cumberland, S. A., Harrison, R. M., Allan, J., Young, D. E., Williams, P. I., and Coe, H.:
1225 Receptor modelling of fine particles in southern England using CMB including comparison with
1226 AMS-PMF factors, Atmos. Chem. Phys., 15, 2139-2158, 10.5194/acp-15-2139-2015, 2015.
1227

1228 Young, D. E., Allan, J. D., Williams, P. I., Green, D. C., Flynn, M. J., Harrison, R. M., Yin, J.,
1229 Gallagher, M. W., and Coe, H.: Investigating the annual behaviour of submicron secondary
1230 inorganic and organic aerosols in London, Atmos. Chem. Phys., 15, 6351-6366, 10.5194/acp-15-
1231 6351-2015, 2015a.
1232

1233 Young, D. E., Allan, J. D., Williams, P. I., Green, D. C., Harrison, R. M., Yin, J., Flynn, M. J.,
1234 Gallagher, M. W., and Coe, H.: Investigating a two-component model of solid fuel organic aerosol
1235 in London: processes, PM1 contributions, and seasonality, Atmos. Chem. Phys., 15, 2429-2443,
1236 10.5194/acp-15-2429-2015, 2015b.

1237

1238 Zhang, Q., Jimenez, J. L., Canagaratna, M. R., Allan, J. D., Coe, H., Ulbrich, I., Alfarra, M. R.,
1239 Takami, A., Middlebrook, A. M., Sun, Y. L., Dzepina, K., Dunlea, E., Docherty, K., DeCarlo, P.
1240 F., Salcedo, D., Onasch, T., Jayne, J. T., Miyoshi, T., Shimono, A., Hatakeyama, S., Takegawa,
1241 N., Kondo, Y., Schneider, J., Drewnick, F., Borrmann, S., Weimer, S., Demerjian, K., Williams,
1242 P., Bower, K., Bahreini, R., Cottrell, L., Griffin, R. J., Rautiainen, J., Sun, J. Y., Zhang, Y. M., and
1243 Worsnop, D. R.: Ubiquity and dominance of oxygenated species in organic aerosols in
1244 anthropogenically-influenced Northern Hemisphere midlatitudes, Geophysical Research Letters,
1245 34, Artn L13801 Doi 10.1029/2007gl029979, 2007.
1246

1247 Zhang, Q., Jimenez, J. L., Canagaratna, M. R., Ulbrich, I. M., Ng, N. L., Worsnop, D. R., and Sun,
1248 Y. L.: Understanding atmospheric organic aerosols via factor analysis of aerosol mass
1249 spectrometry: a review, Anal Bioanal Chem, 401, 3045-3067, DOI 10.1007/s00216-011-5355-y,
1250 2011.
1251

1252 Zhao, R., Lee, A. K. Y., Huang, L., Li, X., Yang, F., and Abbatt, J. P. D.: Photochemical processing
1253 of aqueous atmospheric brown carbon, Atmos. Chem. Phys., 15, 6087-6100, 10.5194/acp-15-
1254 6087-2015, 2015.

1255

1256

1257

1258

1259

1260

1261

1262

1263

1264

1265

1266

Figure Captions

1269   Fig. 1. Geographical locations of the sampling sites (i.e., North Kensington and Detling) in this
1270   study. The region circled by the M25 motorway is the greater London area. The map is adapted
1271   from Google Maps.

1272   Fig. 2. Scatter plot of converted volume (based on HR-ToF-AMS total + BC + crustal material)
1273   vs. the apparent volume estimated from SMPS measurement for (a) the bypass line and the TD
1274   line at (b) 120°C and (c) 250°C. The composition-dependent CE is applied to the bypass line HR-
1275   ToF-AMS measurements and CE = 0.45 is applied to the TD line HR-ToF-AMS measurements.
1276   The slopes and intercepts are obtained by orthogonal distance regression (ODR). The Pearson's R
1277   is obtained by linear least-squares fit.

1278   Fig. 3. (a) Time series of non-refractory species and black carbon in addition to the flag waves of
1279   dominant air mass origin based on the NAME model. (b) Average concentration of non-refractory
1280   species, black carbon, and OA factors resolved by PMF analysis for the easterly sector, westerly
1281   sector, and the whole campaign. The unexplained mass by PMF analysis is less than 6% of total
1282   OA and not shown in the figure. The gap between 1/22 and 1/25 is due to a clogged instrument
1283   inlet.

1284   Fig. 4. (a) Time series of OA factors resolved from the unconstrained PMF analysis on the ambient
1285   data (i.e. $PMF_{ambient}$) and corresponding external tracers. (b) Mass spectra of OA factors, which
1286   are colored by the ion type. The time series of total nitrated phenols is from Mohr et al. (2013).

1287   Fig. 5. f_{44} vs. f_{43} for Detling and NK sites, as well as for the westerly sector and easterly sector of
1288   the Detling site. The dotted lines were adapted from Ng et al. (2010). The averages are sized by
1289   average organic loading. The error bars indicate one standard deviation. The average OA
1290   concentration at the Detling site is different from the value in Fig. 3 due to different sampling
1291   periods.

1292   Fig. 6. Comparison between NK and Detling sites in terms of the campaign-averaged concentration
1293   and mass fraction of non-refractory species and OA factors. The unexplained mass by PMF
1294   analysis is less than 6% of total OA and not shown in the figure.

1295   Fig. 7. Comparison of non-refractory species time series between NK and Detling sites. The
1296   intercept and slope are obtained by orthogonal distance regression. The Pearson's R is obtained by
1297   linear least-squares fit.

1298   Fig. 8. Comparison of OA factors time series between NK and Detling sites. The intercept and
1299   slope are obtained by orthogonal distance regression. The Pearson's R is obtained by linear least-
1300   squares fit.

1301   Fig. 9. Thermogram of (a) non-refractory species and (b) OA factors. The change in mass
1302   concentration after heating in the TD (i.e., ΔC) of (c) non-refractory species and (d) OA factors.

1303 Error bars indicate one standard deviation. The average values are connected by lines to guide the
1304 eyes.

1305 Fig. 10. Mass fraction of PM_1 species for bypass line and TD line (i.e., 120°C and 250°C). The
1306 mass fractions larger than 9% are labeled in the figure.

1307 Fig. 11. Comparison between organics associated with rBC (measured by SP-AMS with laser
1308 vaporizer only) and the non-refractory organics in the bulk measurement (by HR-ToF-AMS) after
1309 heating at 250°C.

1310 Fig. 12. (a) Organic mass fraction remaining (MFR) and O:C as a function of TD temperature; (b)
1311 − (e) organic MFR at 120°C and 250°C as a function of bypass line organic O:C and oxidation
1312 state.

1313 Fig. 13. The properties (O:C and volatility) of three model compounds and the composition of two
1314 populations of particles used in the simple model to illustrate the relationship between bulk OA
1315 O:C and volatility. The O:C is 1, 0.5, and 0.1 for compound A, B, and C, respectively. Upon
1316 heating at temperature T0, 50%, 65% and 100% of A, B, and C would evaporate. Population #1 is
1317 comprised of 0.25, 0.7, and 0.05 µg m^{-3} of A, B, and C, respectively, and population #2 is
1318 comprised of 0.7, 0.05, and 0.25 µg m^{-3} of A, B, and C, respectively.

1319 Fig. 14. (a) O:C enhancement (i.e., ratio of TD line O:C to bypass line O:C) as a function of bypass
1320 line O:C. (b) Mass spectra of OA under different TD temperatures. The signals between *m/z* 45
1321 and 99 are multiplied by 10 and the signals between *m/z* 100 and 150 are multiplied by 25 for
1322 clarity. The mass spectra are colored by the ion type in the same way as Fig. 4b.

1323
1324
1325
1326
1327
1328
1329
1330
1331
1332
1333
1334
1335
1336
1337
1338
1339
1340

1341   Fig. 1
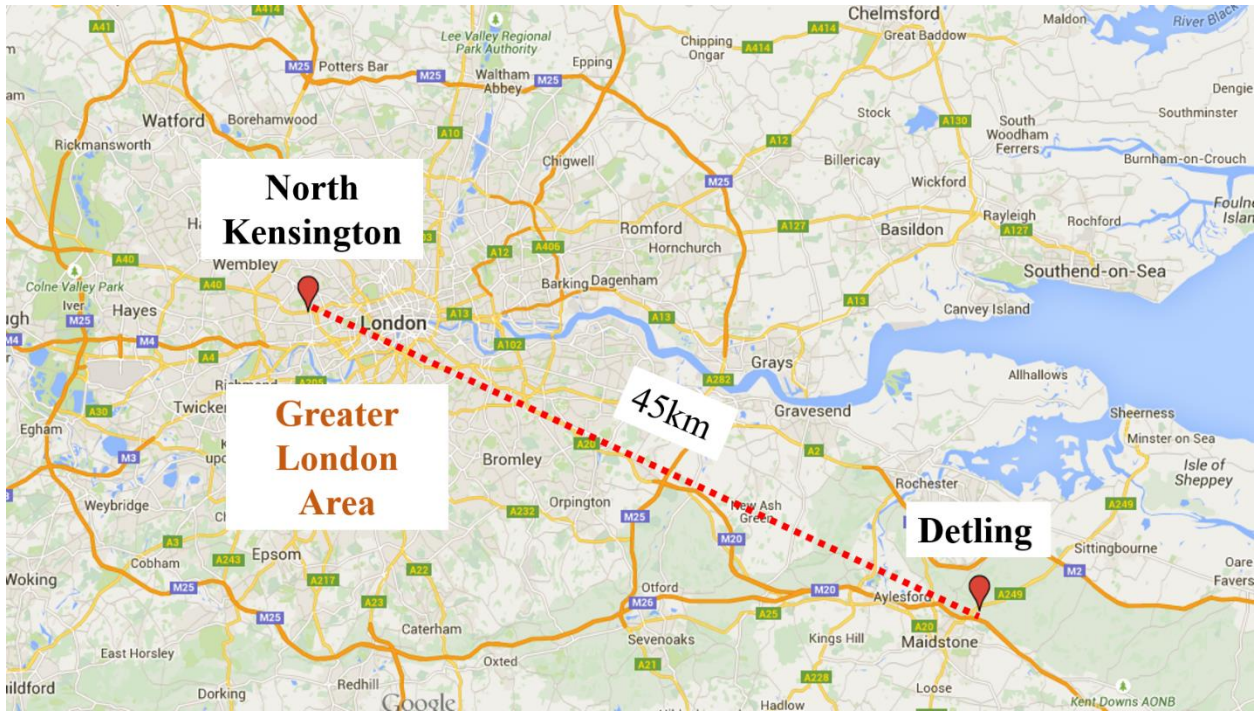
1342
1343
1344
1345
1346
1347
1348
1349
1350
1351
1352
1353
1354
1355
1356
1357
1358
1359
1360
1361
1362
1363
1364
1365

1366   Fig. 2
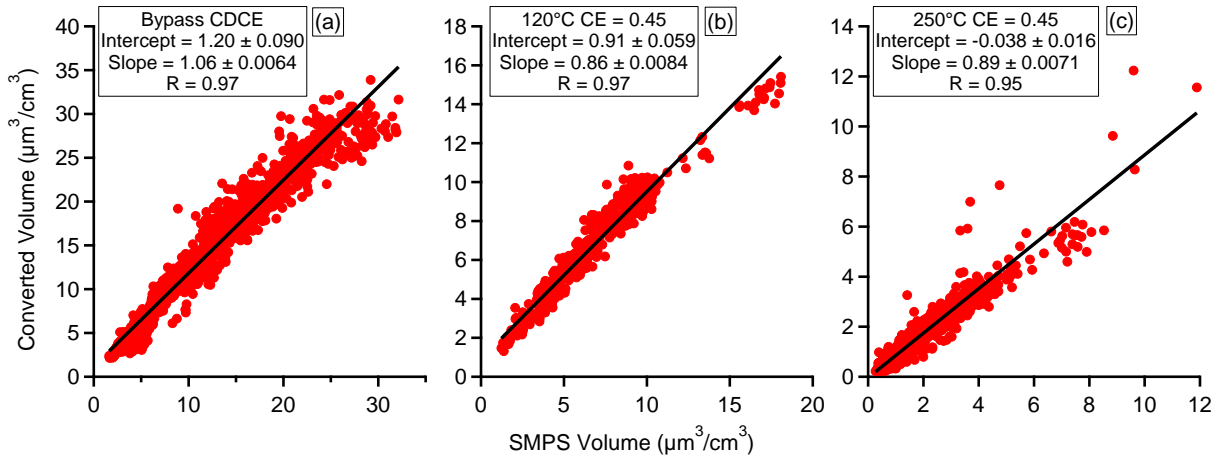
1367
1368
1369
1370
1371
1372
1373
1374
1375
1376
1377
1378
1379
1380
1381
1382
1383
1384
1385
1386
1387
1388
1389
1390
1391
1392
1393
1394
1395
1396

1397   Fig. 3
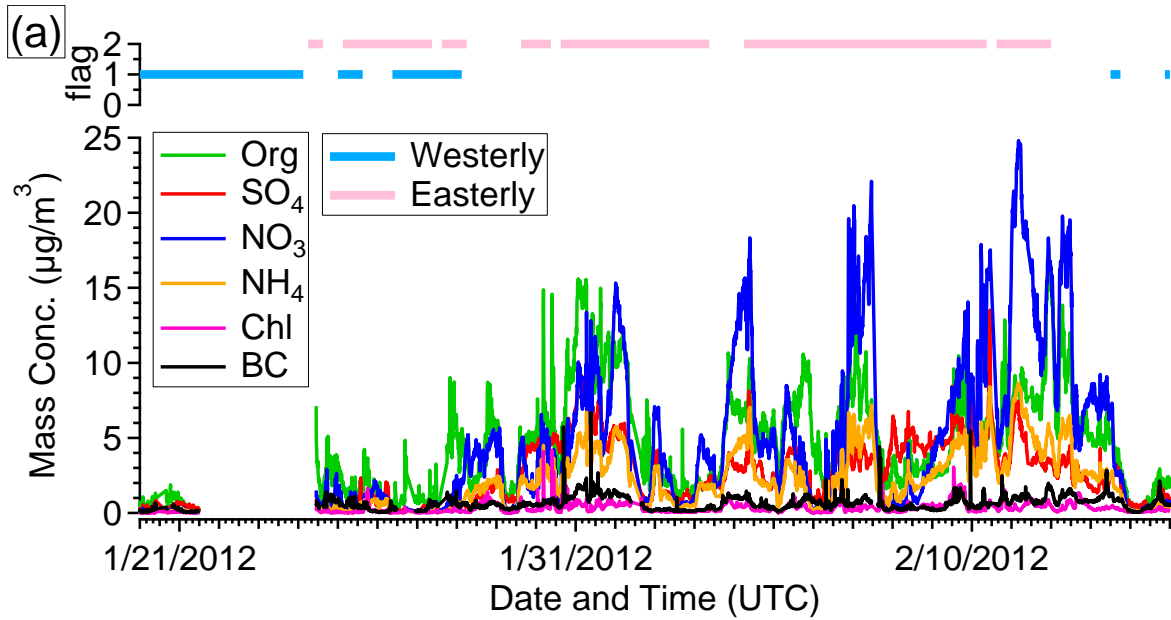
1398
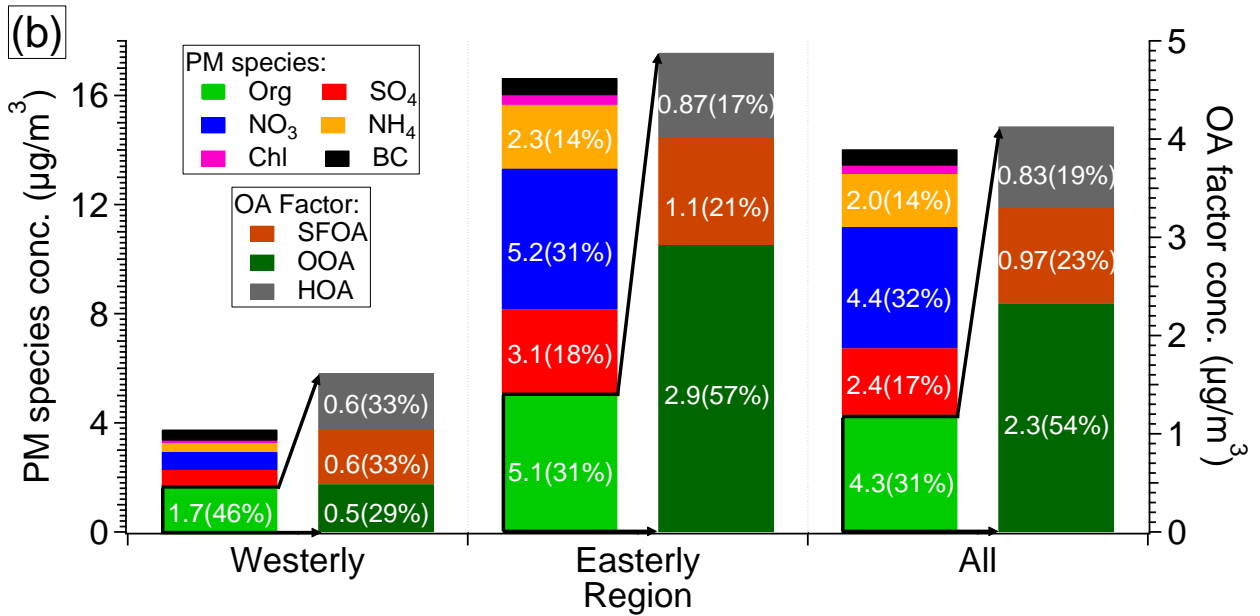
1399
1400
1401
1402
1403
1404
1405
1406
1407
1408
1409

1410   Fig. 4
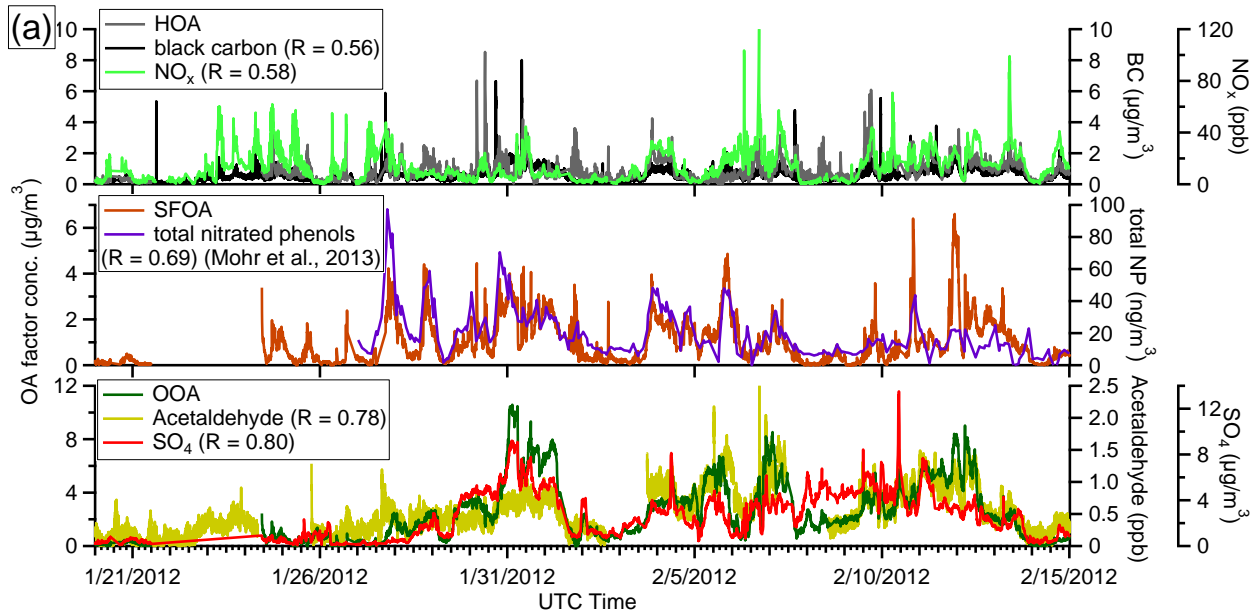
1411
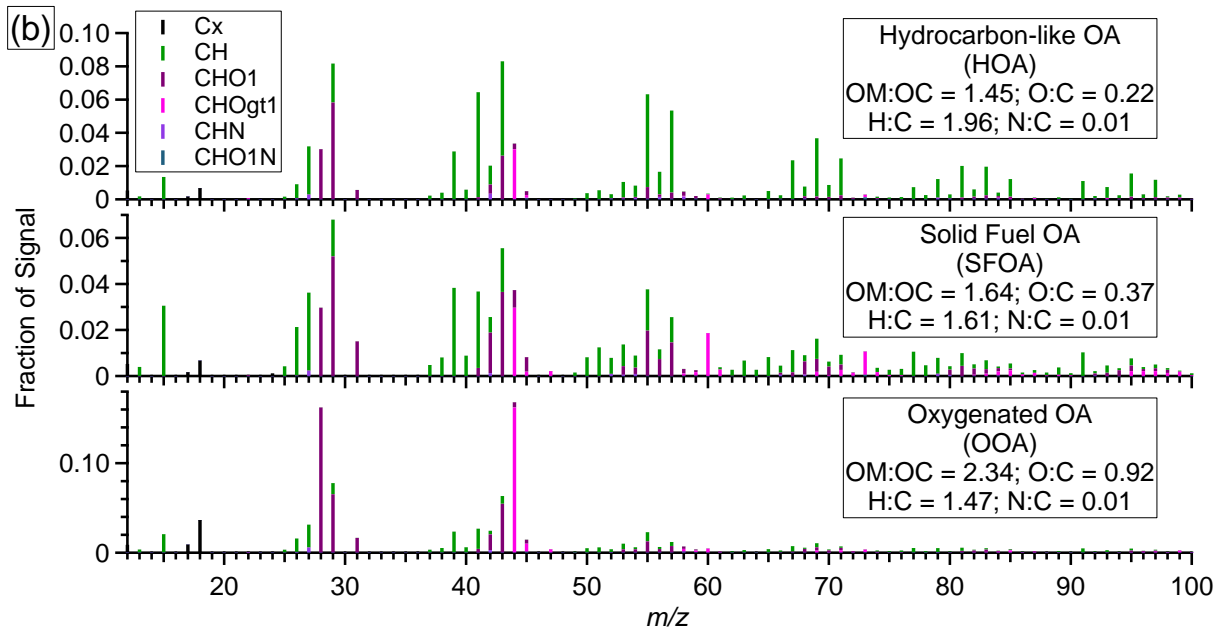
1412
1413
1414
1415
1416
1417
1418
1419
1420
1421
1422
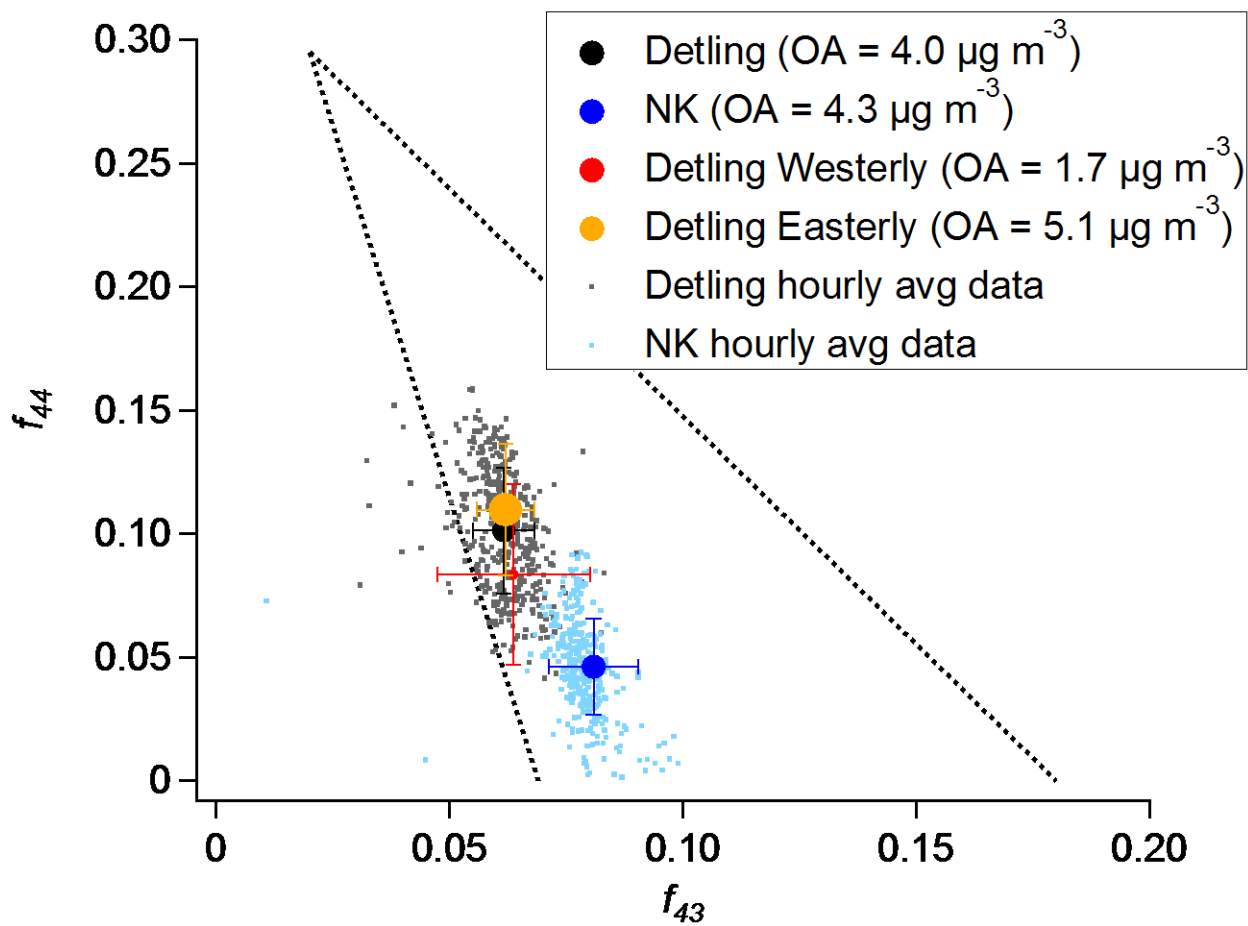
1424
1425
1426
1427
1428
1429
1430
1431
1432
1433
1434
1435
1436
1437
1438
1439
1440
1441

1442   Fig. 6
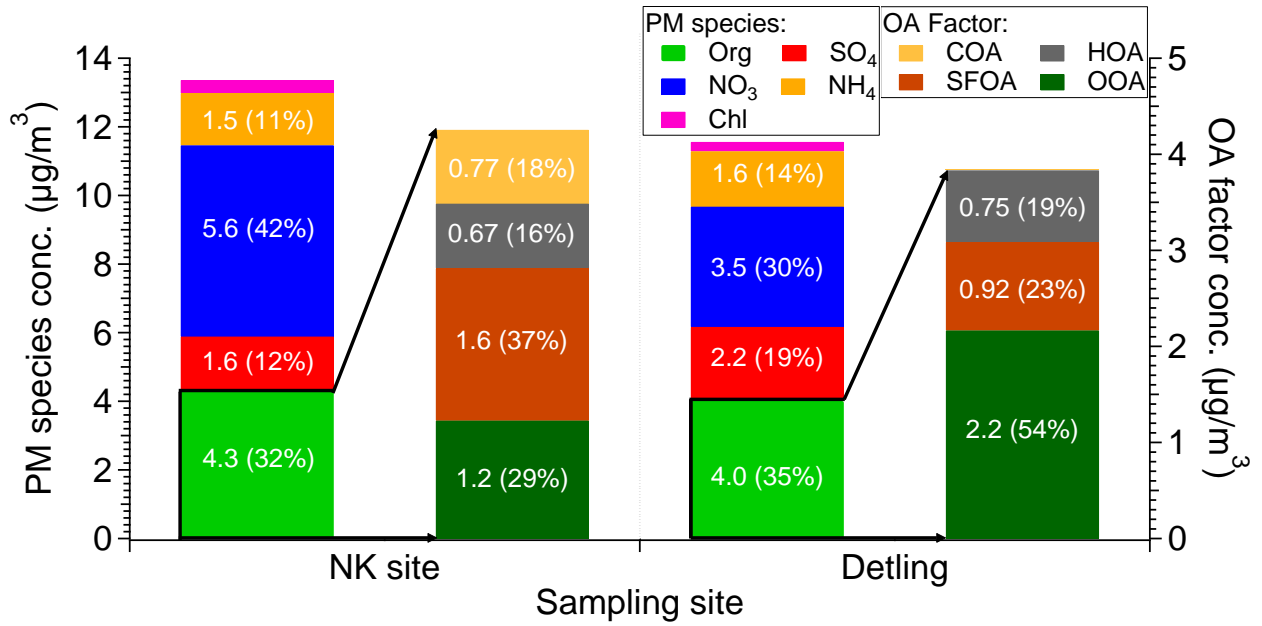
1443
1444
1445
1446
1447
1448
1449
1450
1451
1452
1453
1454
1455
1456
1457
1458
1459
1460
1461
1462
1463
1464
1465
1466
1467

1468   Fig. 7.

1469
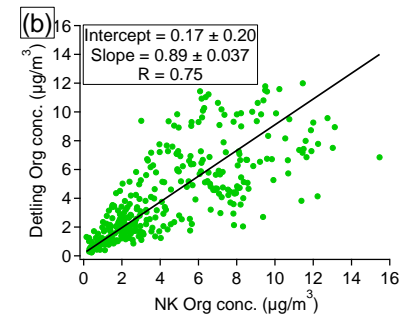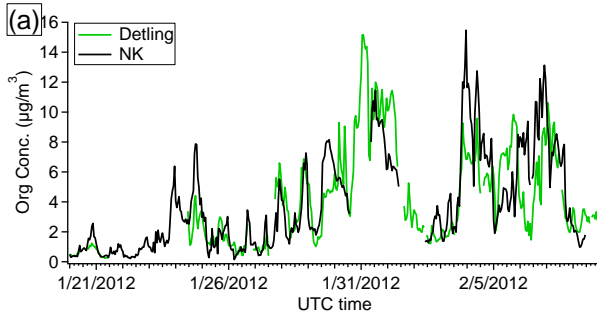
1470
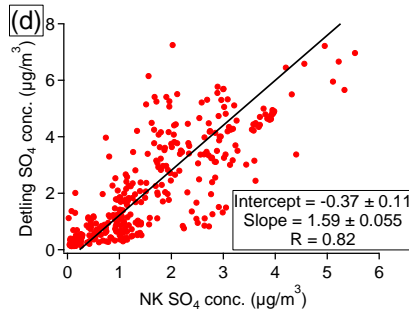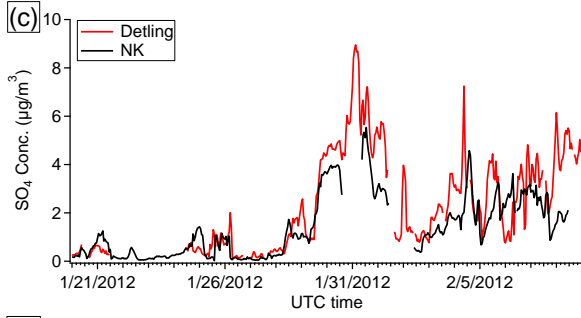
1471
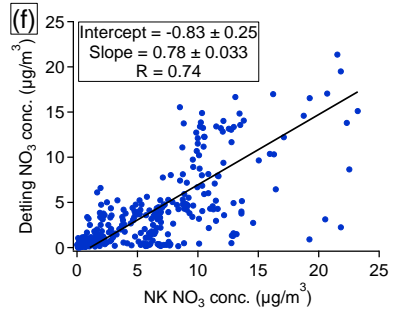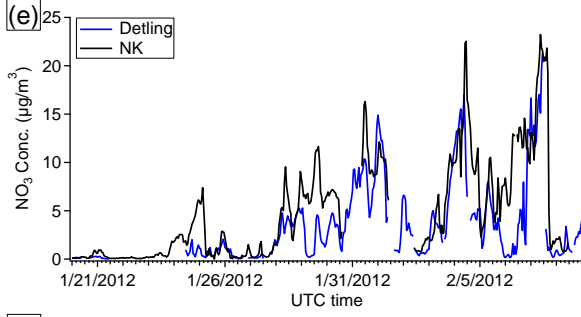
1472
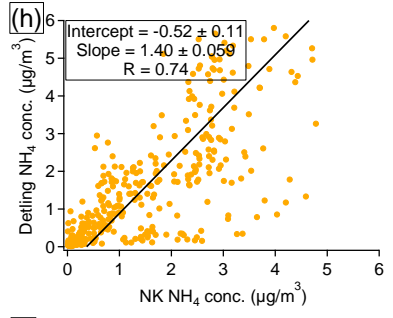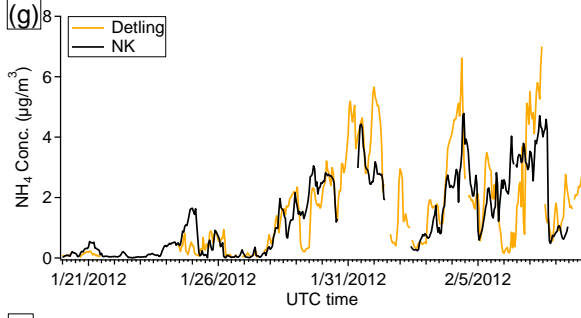
1473
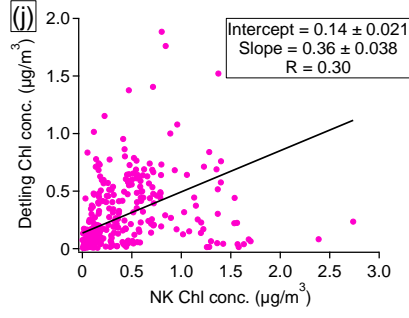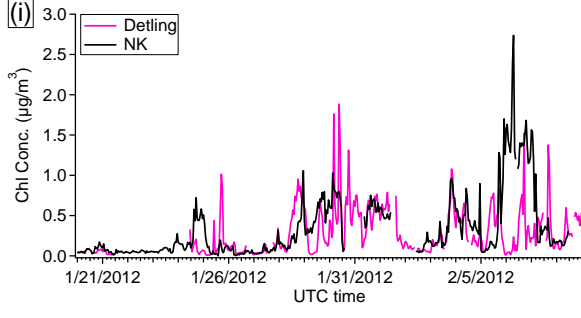
1474

1475   Fig. 8
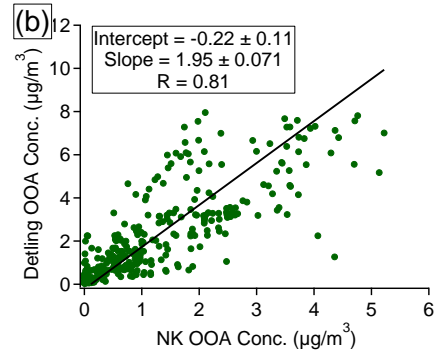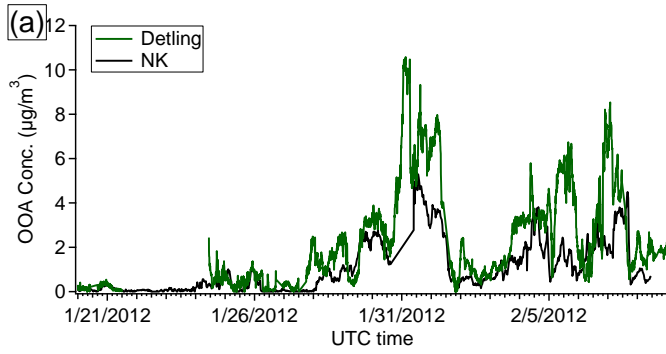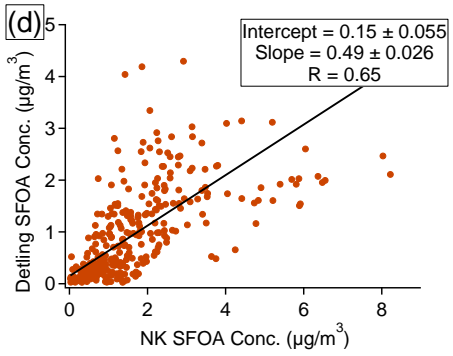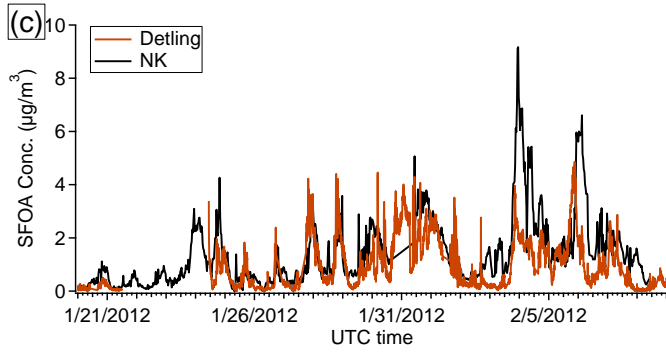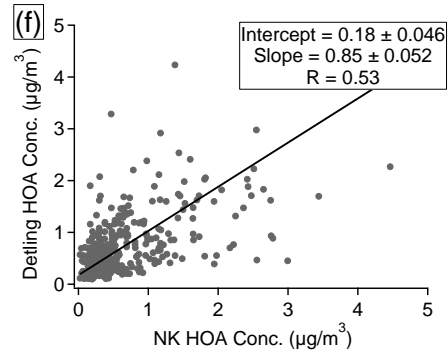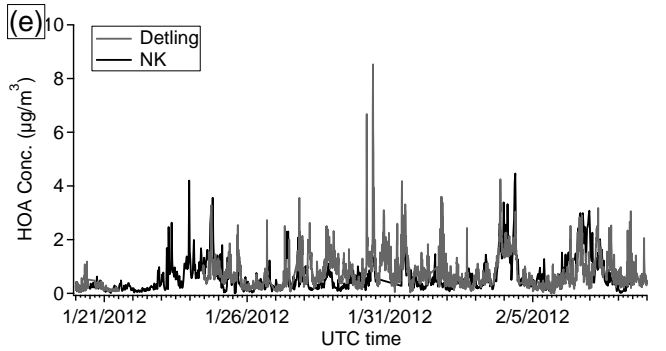
1486   Fig. 9
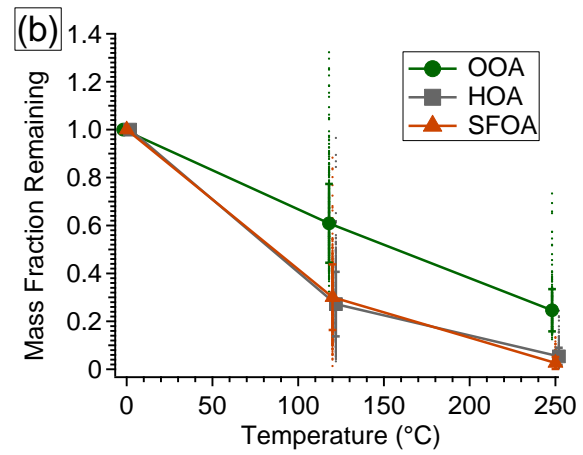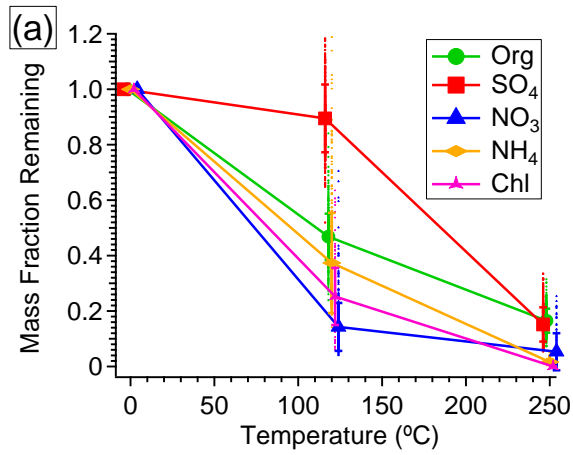
1487
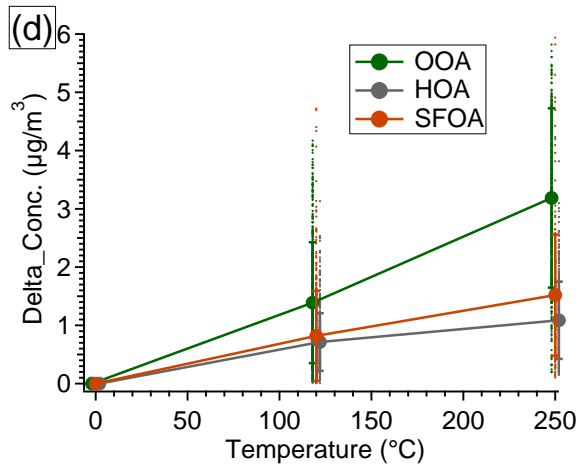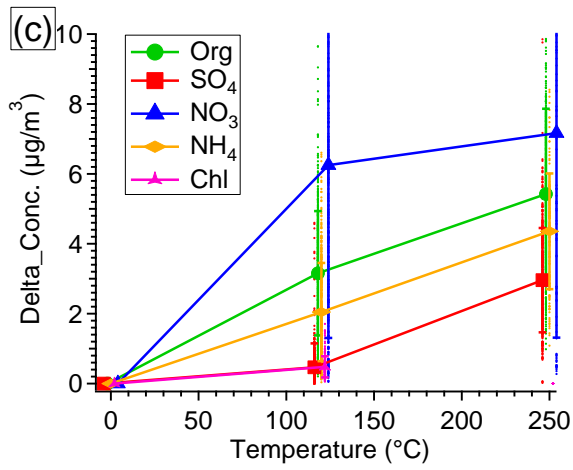
1488
1489
1490
1491
1492
1493
1494
1495
1496
1497
1498
1499
1500
1501
1502
1503
1504
1505
1506

1507   Fig. 10
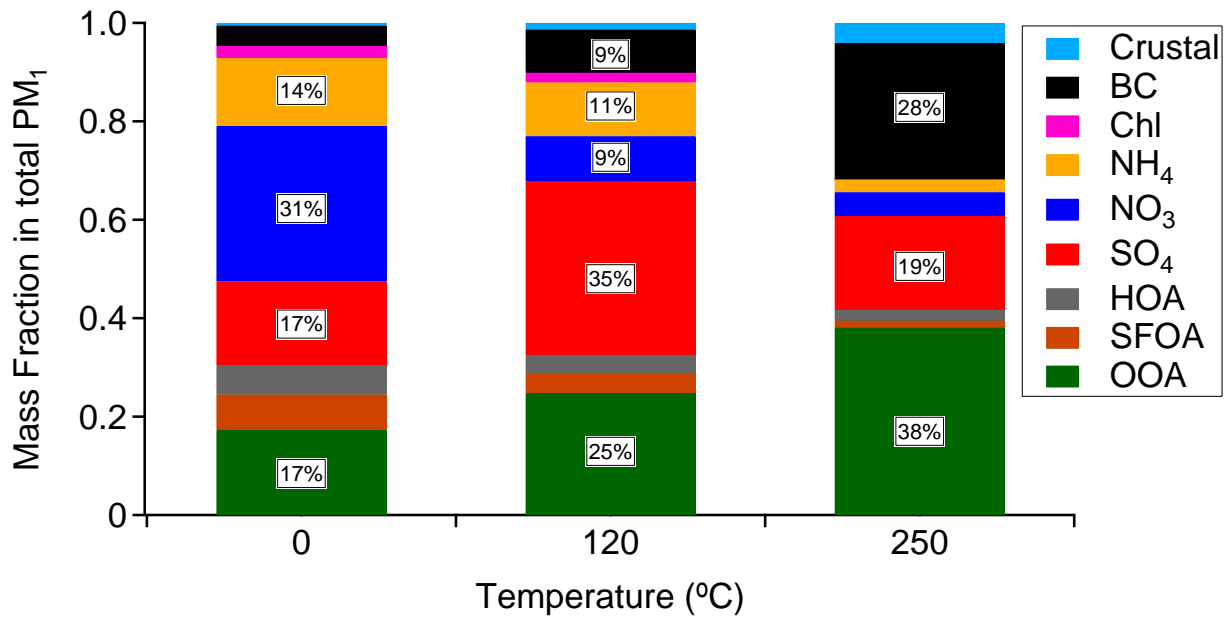
1508
1509
1510
1511
1512
1513
1514
1515
1516
1517
1518
1519
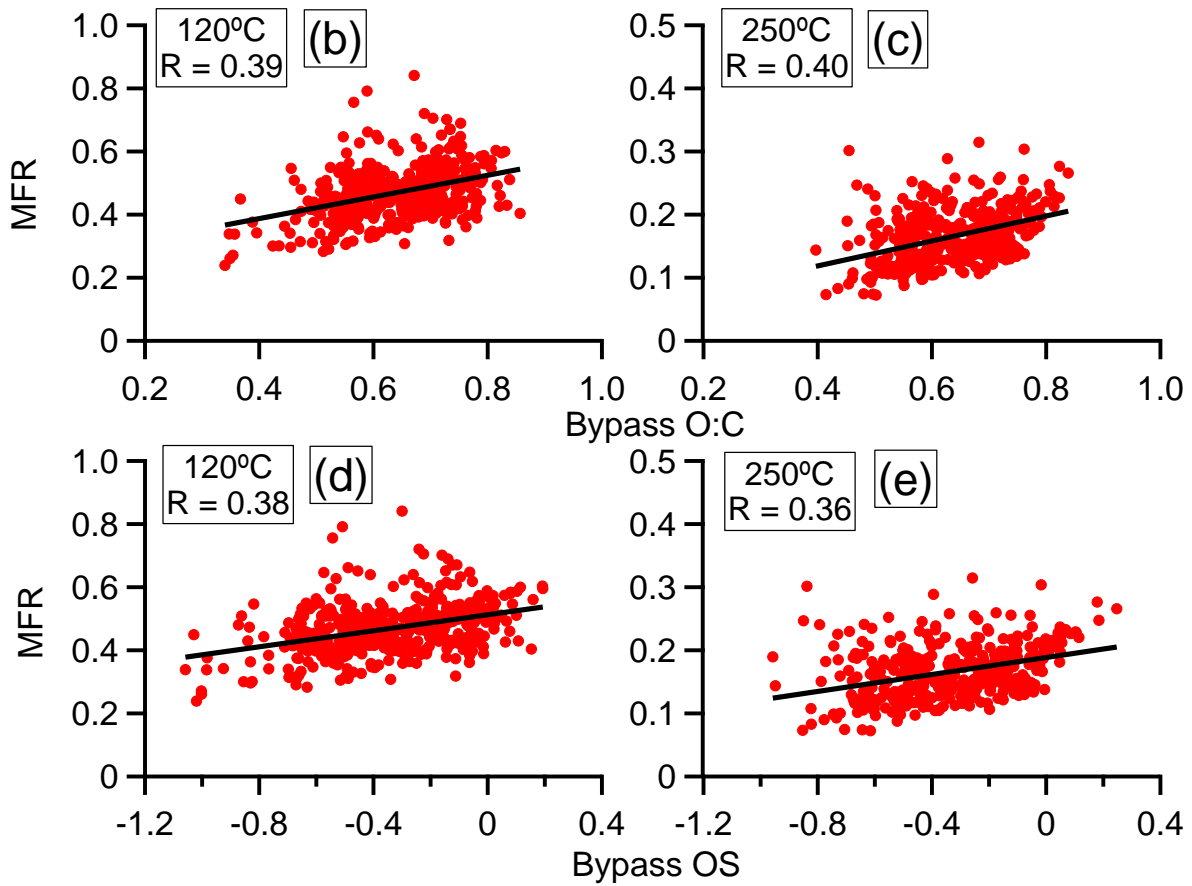1520
1521
1522
1523
1524
1525
1526
1527
1528
1529
1530
1531
1532

Fig. 11
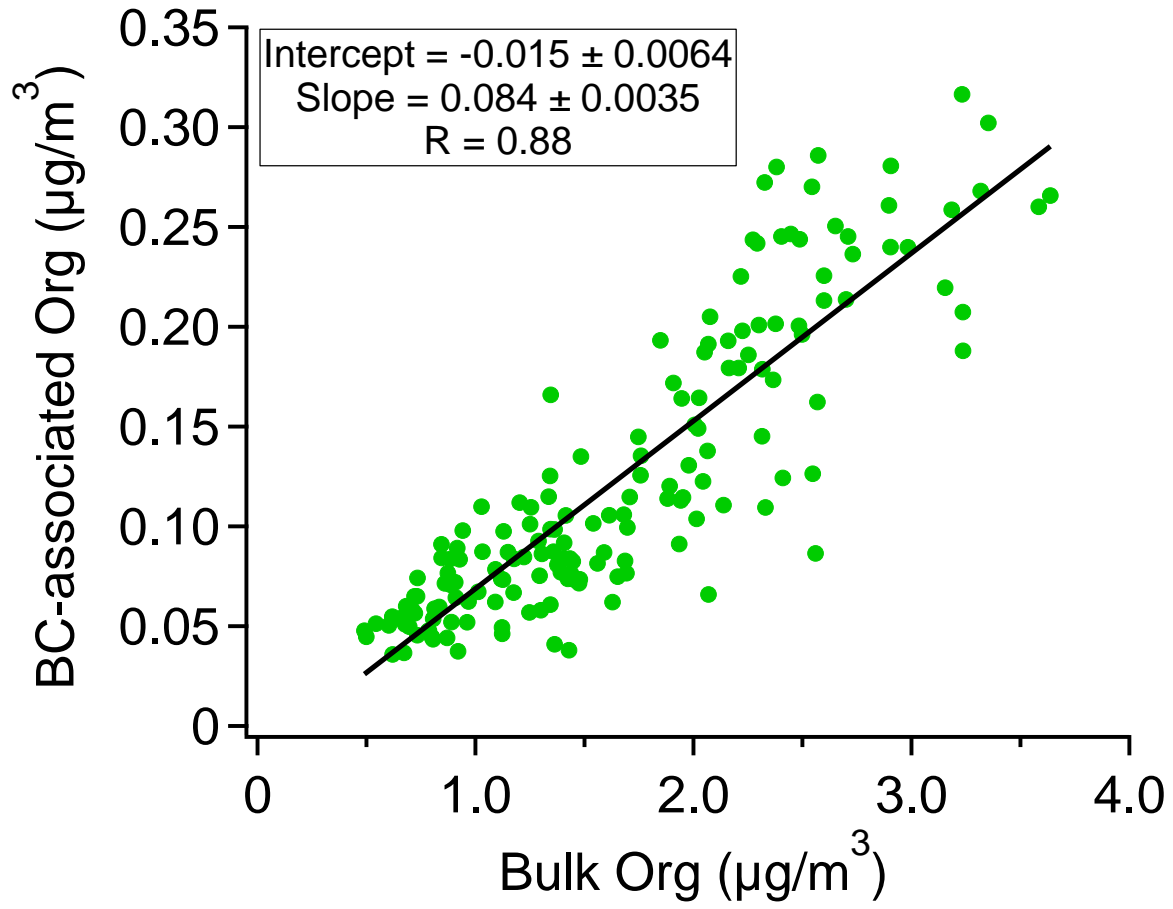
1534
1535
1536
1537
1538
1539
1540
1541
1542
1543
1544
1545
1546
1547
1548
1549
1550
1551

1552   Fig. 12
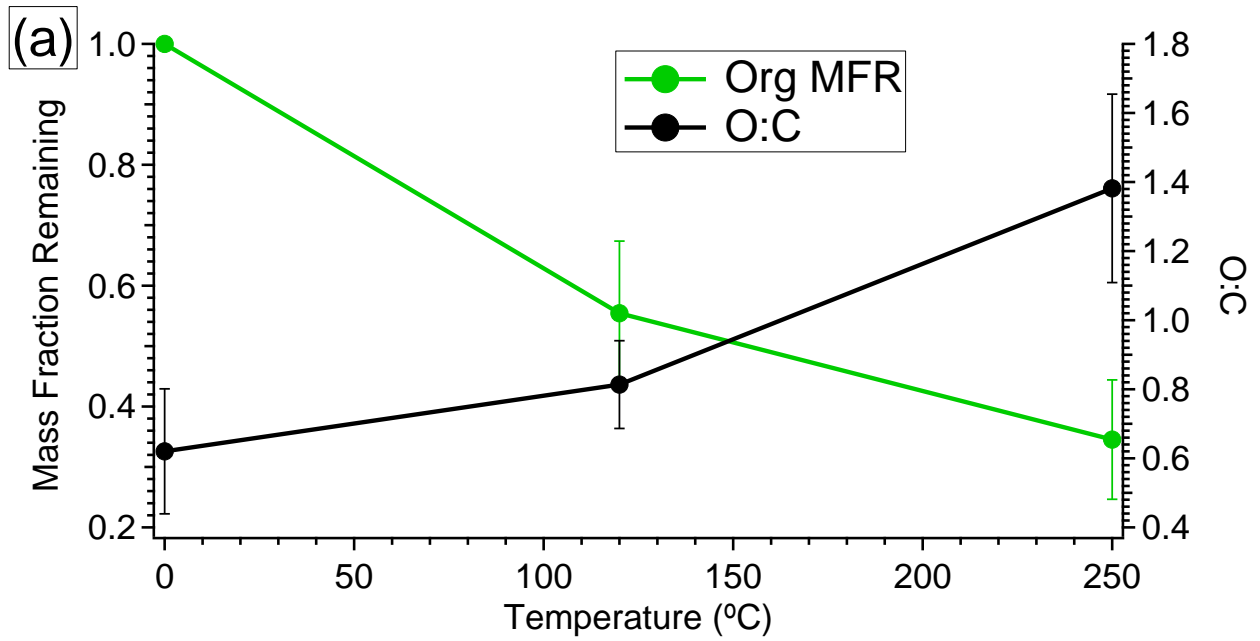
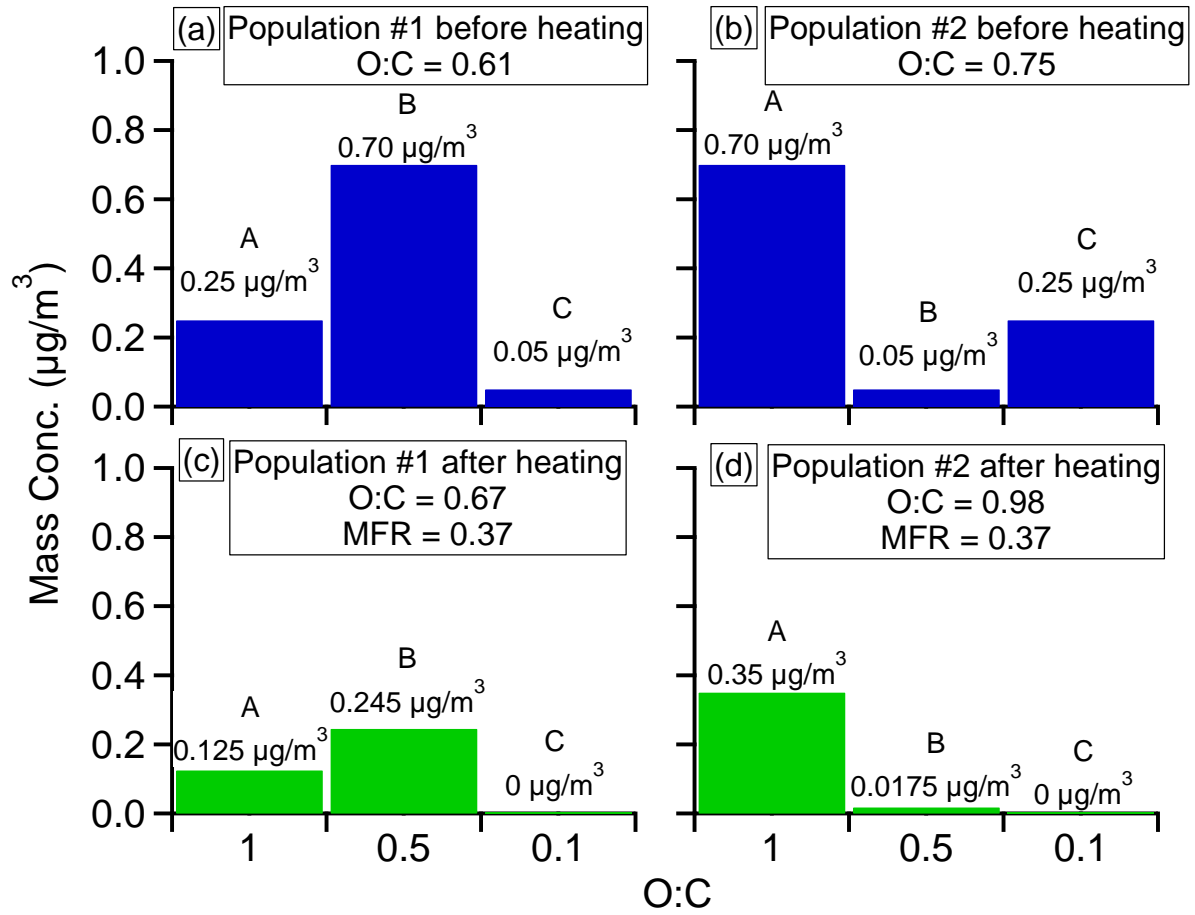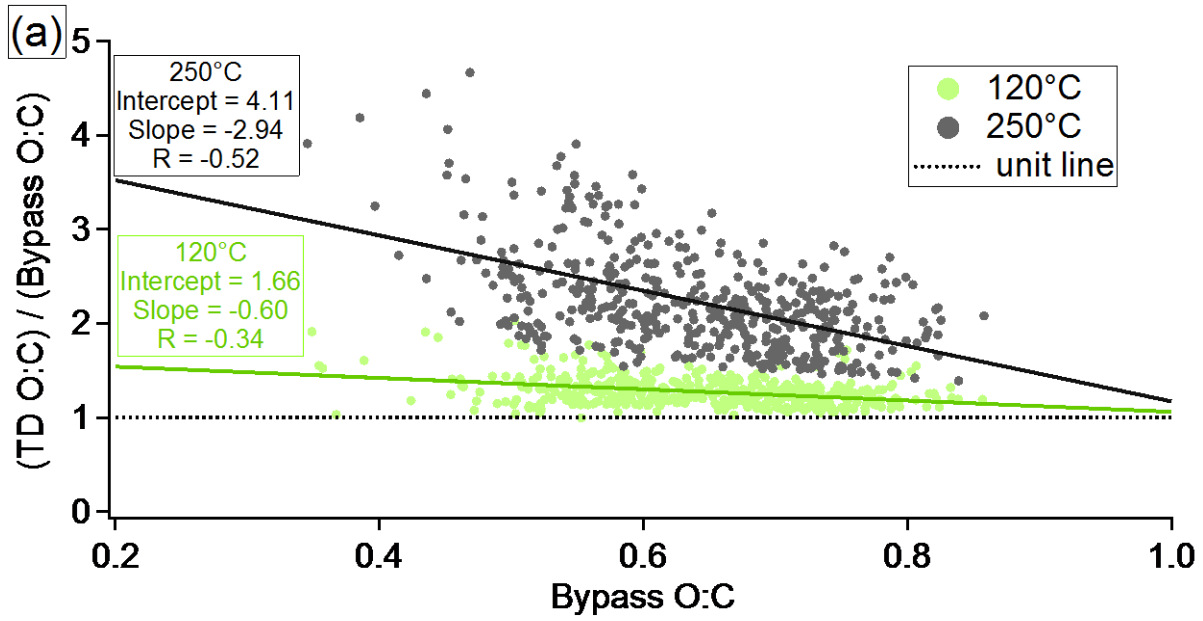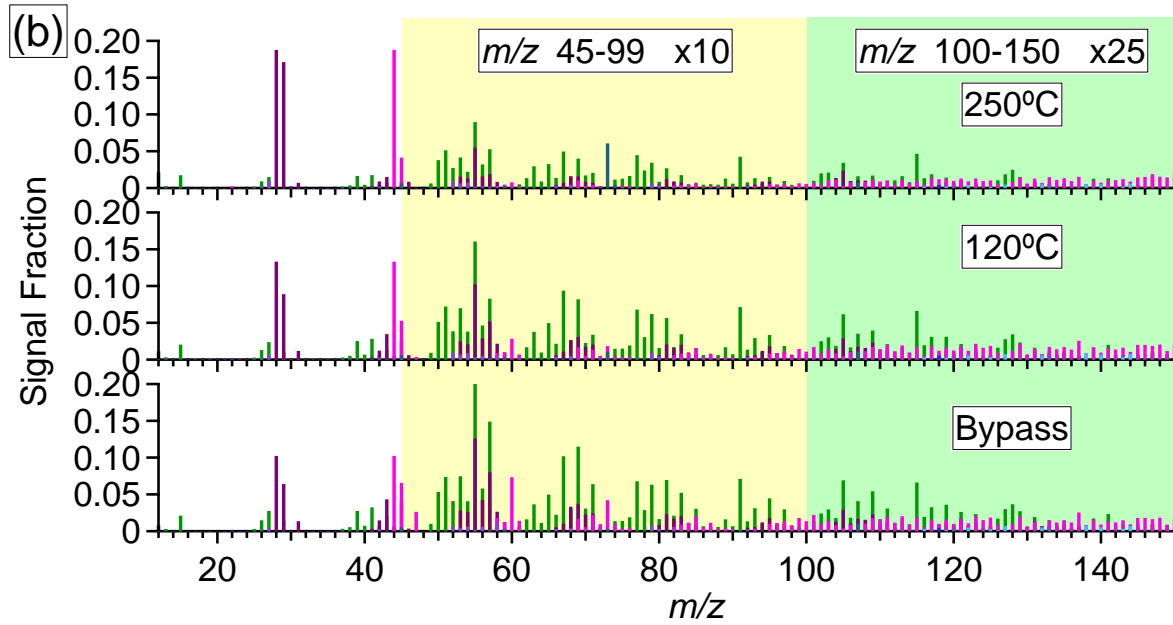

1553

1554
1555
1556
1557

1577   Fig. 14

(a)

250°C
Intercept = 4.11
Slope = -2.94
R = -0.52

120°C
Intercept = 1.66
Slope = -0.60
R = -0.34

- 120°C
- 250°C
······· unit line

(TD O:C) / (Bypass O:C)

Bypass O:C

1578

(b)

m/z 45-99   x10   m/z 100-150   x25
250ºC

120ºC

Bypass

Signal Fraction

m/z

1579

1580